

Deep Learning Framework for Urban Impervious Surface Mapping Using Open Multisource Geospatial Data

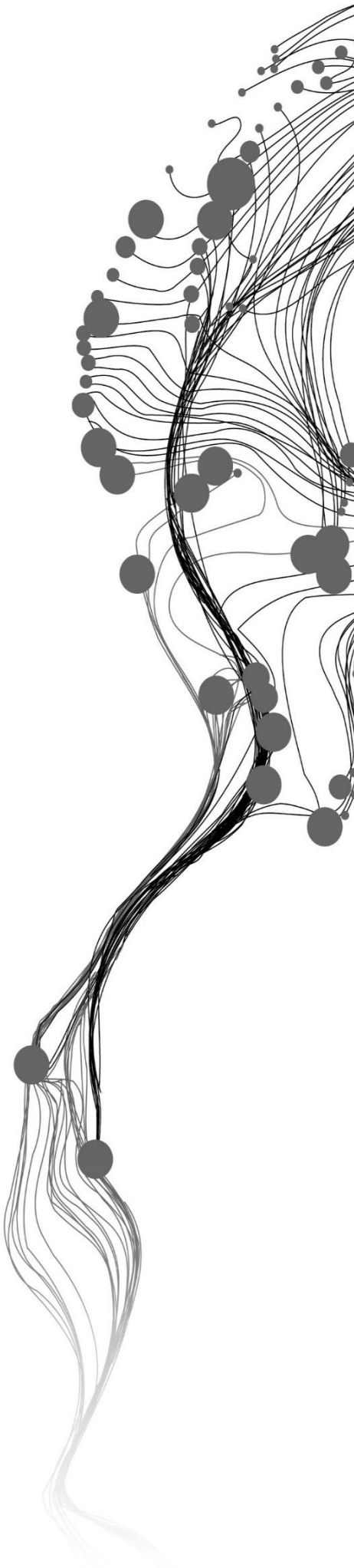
SHANMATHI BARATHIDHASAN

July, 2023

SUPERVISORS:

Dr., Mahdi Khodadadzadeh

Dr., Mahdi Farnaghi



A Deep Learning Framework for Urban Impervious Surface Mapping Using Open Multisource Geospatial Data

SHANMATHI BARATHIDHASAN

Enschede, The Netherlands, July, 2023

This thesis is submitted to the Faculty of Geo-Information Science and Earth Observation of the University of Twente in partial fulfillment of the requirements for the degree of Master of Science in Geo-information Science and Earth Observation.

Specialization: Geoinformatics

SUPERVISORS:

Dr. Mahdi Khodadadzadeh

Dr. Mahdi Farnaghi

THESIS ASSESSMENT BOARD:

Chair: Prof. Dr. Menno-Jan Kraak

External Examiner: Dr. Raian Vargas Maretto

Procedural advisor: Dr. rer.nat. Franz-Benjamin Mocnik

Drs. Barend Köbben

DISCLAIMER

This document describes work undertaken as part of a programme of study at the Faculty of Geo-Information Science and Earth Observation of the University of Twente. All views and opinions expressed therein remain the sole responsibility of the author, and do not necessarily represent those of the Faculty.

ABSTRACT

Developing a comprehensive understanding of urbanization and the urban ecosystem necessitates the requirement of crucial knowledge pertaining to Urban Impervious Surfaces (UIS). The need for an updated and accurate classification of UIS is of growing importance. Numerous studies have utilized various remote sensing and geospatial data sources to address this need. In this study, we investigate the effective utilization of freely available remote sensing sources, including satellite imagery and Volunteered Geographic Information sources like Twitter and Open Street Map, for UIS classification. An innovative aspect of this research lies in the creative integration of these data sources to acquire UIS training labels required for a Deep Learning based classification system.

We propose a one-class classification approach using Deep One-Class Classification (DOCC) to reduce dependency on labeled data for different classes for an effective UIS classification. The introduced DOCC model demonstrates the efficiency of a deep feature network, utilizing only limited spectral features such as blue, green, and red spectral bands, to achieve accurate UIS classification. The DOCC showed a good accuracy which was later compared with that of a deep multiclass classification, focusing only on UIS class of multiclass. Moreover, the UIS labels proved to be more efficient in comparison to that of the globally available impervious maps.

Overall, this study aims in contributing to the advancement of UIS mapping techniques by integrating various geospatial data sources and exploring innovative classification techniques.

Keywords: Sentinel 2, Volunteered Geographic Information, Twitter, Open Street Map, Urban Impervious Surface, One-Class Classification, Deep feature learning.

ACKNOWLEDGEMENTS

I would like to express my deepest gratitude to Dr. Mahdi Khodadadzadeh, my first supervisor, for his exceptional guidance, invaluable insights, and unwavering support throughout my thesis study. I greatly value his expertise and experience in the field, as they played a vital role in the successful completion of this study. I am sincerely grateful to him for serving as my mentor and imparting invaluable knowledge during this journey.

Furthermore, I would like to take this opportunity to convey my sincere appreciation to Dr. Mahdi Farnaghi, who graciously took on the role of my second supervisor, for providing his insightful recommendations throughout my work. His assistance has significantly contributed to shaping the direction and enhancing the quality of my study.

Furthermore, I am thankful to the chair and esteemed members of the committee for their valuable ideas, insightful comments, and constructive criticism. Their input and feedback have played a pivotal role in shaping the outcomes of my study, and I am grateful for the opportunity to benefit from their knowledge and expertise.

Special thanks are also due to the procedural advisors who have provided invaluable support in managing the various tasks associated with my thesis. Their guidance and assistance have greatly facilitated the administrative aspects of my research, enabling me to focus on the core elements of my study.

To conclude, but by no means least, I would want to express my heartfelt thanks to my family and friends for their unwavering support, guidance, and understanding throughout my academic journey. Their constant presence and encouragement have been a source of strength and inspiration, empowering me to overcome challenges and achieve my goals. I am truly grateful for their unconditional love, support, and unwavering belief in my abilities.

TABLE OF CONTENTS

1.	Introduction.....	1
1.1.	Background of the research.....	1
1.2.	Research Identification and Motivation	2
1.3.	Research gap	2
1.4.	Research Objectives and Research Questions	4
1.5.	Thesis Structure	5
2.	Literature Review.....	5
3.	Study area and dataset.....	7
3.1.	Selected study Area	7
3.2.	Datasets considered for the study	8
4.	Methodology.....	10
4.1.	Acquiring Quality data.....	10
4.2.	Deep learning model for Impervious surface detection and mapping	14
4.2.1	Deep One-class Classification.....	14
4.2.2	Deep Multi-class Classification.....	19
4.2.3	Comparison with the existing Global Impervious Map	19
5.	Results and discussions.....	20
5.1	Results and dicussion on Deep One-Class Classification (DOCC)	20
5.2	Results and discussion on Deep Multi-class Classification.....	24
5.3	Comparison between One-class classifier and Multi-class classifier.....	25
5.4	Results and dicussion on Comparison of acquired UIS map with existing Global map.....	26
6.	Conclusions.....	27
6.1	Conclusion.....	27
6.2	Research Limitations and future works.....	29
7.	Ethical Considerations, risks, and Contingencies.....	29

LIST OF FIGURES

Figure 1 Study Area Map.....	7
Figure 2 Map depicting the geographical locations of user tweets.	9
Figure 3 Flowchart representing the methodology of pre-processing.....	10
Figure 4 Tweets within the waterbodies and forest areas.....	11
Figure 5 A buffer created around one of the selected tweets (left) and the tweet reduction after selection process (right)	11
Figure 6 Flowchart representing the methodology of this study.....	12
Figure 7 Map of selected tweets after pre-processing.....	13
Figure 8 Sample patch acquired through the proposed pipeline	13
Figure 9 Code snippet of the shape of training and testing datasets	14
Figure 10 Summary of the Model architecture	16
Figure 11 Workflow of training phase.....	17
Figure 12 Workflow of testing Phase	18
Figure 13 Representation and formula for the evaluation metrics (Ma et al., 2019)	18
Figure 14 Graph showing initial loss versus epoch	20
Figure 15 Graph showing loss versus epoch after changes in loss function	20
Figure 16 Graph showing loss versus epoch after hyperparameter tuning.....	21
Figure 17 Graph depicting predicted scored versus true labels	22
Figure 18 Confusion matrix for DOCC.....	23
Figure 19 Detection by the DOCC model.....	23
Figure 20 Confusion matrix output from second phase of testing.....	24
Figure 21 Graph on evaluation metrics for each epoch	24
Figure 22 Confusion Matrix for multi-class classification.....	25
Figure 23 Comparison between GISA and UIS at 10 m resolution	27

LIST OF TABLES

Table 1 Spectral bands of Sentinel 2 utilized for this study	9
Table 2 Reference and Target Dataset split	14
Table 3 Evaluation metrics of both DOCC and DMCC	25

LIST OF ACRONYMS

UIS	Urban impervious surface
DOCC	Deep One-Class Classification
VGI	Volunteered Geographic Information
OSM	Open Street Maps
CNN	Convolution Neural Network
OVSVM	One-Class Classification through Support Vector Machine
GPS	Global Positioning System
NDVI	Normalized difference vegetative Index
NDWI	Normalized difference water Index
NDBI	Normalized difference Built-up Index
SAR	Synthetic Aperture Radar
OCSVM	One-Class Classification Support Vector Machine
BSVM	Biased Support Vector Machine
PUL	Positive-Unlabelled Learning
PBL	Presence and Background learning
MAXENT	Maximum Entropy Model
UAV	Unmanned Aerial Vehicle
GMIS	Global Man-made Impervious Surface map and Settlement extent
GISA	Global Impervious Surface Area
DMCC	Deep Multi-Class Classification
ESA	European Space Agency
NASA	National Aeronautics and Space Administration
LIDAR	Light Detection and Ranging
MSI	Multi-Spectral Imaging
CRS	Co-ordinate Reference System

1. INTRODUCTION

1.1. Background of the research

Urban Impervious Surface (UIS) denotes artificial structures and surfaces within urban areas that directly impede water infiltration into the ground (Y. Wang & Li, 2022). In urban environments, UIS includes a range of human-made structures such as roads, parking lots, sidewalks, rooftops, and paved surfaces. It is commonly regarded as a prominent indicator of urban area expansion, urban growth, and an increase in human settlements in urban areas (Arnold & Gibbons, 1996). In recent times, notable advancements have been achieved in the exploration of appropriate geospatial data sources for the mapping of UIS. Here the term mapping refers to the detection of UIS regions by acquiring specific labels denoting the existence of the imperviousness in the region (Parekh et al., 2021).

Data fusion is an emerging scientific research concept that encompasses the amalgamation of data from diverse sources to generate a cohesive solution or produce visually appealing high-quality representations of the data (Hall et al., 1997; Khaleghi et al., 2013; Schmitt & Zhu, 2016; Zhang, 2010). In the domain of remote sensing, research includes merging satellite imagery with airborne data, with the primary objective of extracting comprehensive and detailed information (Zhang, 2010). One of the key objectives of this study is to investigate the concept of fusing multiple geospatial data, specifically integrating satellite imagery and Volunteered Geographic Information (VGI) data, within the fields of remote sensing and Geographic Information Science (GIS). The utilization of openly and freely accessible multiple data sources renders them readily available and cost-effective.

Satellite imagery is frequently utilized as the predominant geospatial data source in the domain of remote sensing. Nevertheless, in terms of UIS mapping, supportive data sources such as VGI play a pivotal role. VGI refers to user-generated information, which includes text and multimedia, that provides geographical information (Devkota et al., 2019). This study proposes an approach to integrate satellite imagery with supportive VGI data, specifically from Twitter and Open Street Map (OSM) to detect UIS regions.

This study allows for the classification of UIS regions using the above-mentioned geospatial data without being constrained by factors like label acquisition costs, computational time, and the need for extensive manual work. To accomplish this objective, the study suggests employing a technique based on One-Class Classification (OCC) and utilizing deep learning techniques like Convolutional Neural Networks (CNN). The proposed Deep One-Class Classification (DOCC) framework helps to enhance the efficiency of UIS mapping while minimizing manual efforts and addressing associated constraints.

Hence, alongside exploring data fusion, this project aims to delve into the concept of OCC Deep Learning techniques. The aim is to explore the effective utilization of openly accessible geospatial data, thereby promoting affordability and accessibility for all. Additionally, the Deep Learning OCC technique proposed in this research endeavours to tackle the issue of expensive label acquisition for training purposes and reduce the labour-intensive process of manual labelling or visual interpretation in situations where an adequate number of labels is unavailable.

1.2. Research Identification and Motivation

Urban areas comprise diverse land cover types, including natural elements like parks, forests, and aquatic elements such as ponds and lakes, as well as human-made structures like buildings, parking spaces, and roads. UIS is represented by man-made urban landscape features like concrete and asphalt where percolation does not occur. The presence of these impervious surfaces is crucial in determining the complex dynamics of precipitation and discharge in urban environments (Schoener, 2018).

Furthermore, by acting as a valuable instrument, the study of urban impervious surfaces aids in understanding urban development and expansion while also shedding light on their environmental implications (Sishi Wang et al., 2023). These factors have generated a demand for the latest accurate data on impervious surfaces, which serves as a valuable resource for urban planning and monitoring of urban ecosystems, among other applications.

Traditionally, such information was obtained through field surveys involving GPS technology, which proved time-consuming and labour-intensive. In addition to these conventional techniques, remote sensing techniques are now extensively being used for impervious surface extraction from satellite imagery (Weng, 2012). Over time, remote sensing techniques for detecting impervious surfaces have gained popularity and trust, particularly in combination with Machine Learning classification techniques.

Nowadays, UIS mapping is often carried out by using binary and multiclass classification techniques. These techniques need more land cover class labels. However, acquiring a sufficient number of labelled training examples for each class, which are essential for effective learning, can often be costly. These costs encompass multiple aspects, including the expenses associated with raw data collection, data cleaning efforts, data storage, the procurement of necessary hardware resources utilized for data processing on computers, the time required for learning from the data, the conversion of data into an appropriate format for effective learning purposes, and the opportunity cost which arises from compromised learning outcomes that occur due to a lack of sufficient computational resources for handling extensive datasets (Turney, 2014; Weiss & Provost, 2014).

Thus, finding ways to achieve the study of urban impervious surfaces by integrating traditional and non-traditional open geospatial sources, which are free of cost, with a suitable strategy to counter the concerns of binary or multiclass classifiers to identify such UIS regions could be extremely helpful for future studies and references.

1.3. Research gap

Active research is currently being conducted to acquire labels for impervious surfaces in urban areas, particularly within the domain of remote sensing. The accurate classification of UIS heavily relies on meticulous satellite imagery selection, considering essential factors such as spectral features, spatial resolution, designated time period of the satellite data, and radiometric resolution (Lu et al., 2014). Previous studies have predominantly concentrated on satellites with medium spatial resolution, such as Sentinel and Landsat, which have been extensively employed for research purposes (Fan et al., 2019; Girolamo-Neto et al., 2020; Li, 2020; Sun et al., 2022; Tian et al., 2018).

In addition, there has been significant research on the amalgamation of diverse data sources for the classification and representation of impervious surfaces, including the combination of optical imagery and

SAR (Bai et al., 2019). Significantly few research studies have utilized VGI data, such as OSM, in combination with satellite imagery to extract impervious surfaces (Fan et al., 2019; Z. Miao et al., 2019). Nonetheless, there is negligible research work that effectively combines satellite imagery with VGI sources like social media datasets (e.g., Twitter) and OSM specifically for urban impervious surface mapping (Z. Miao et al., 2019; Parekh et al., 2021; Yan et al., 2018).

The conventional method for mapping UIS (Urban Impervious Surface) involves utilizing spectral indices derived from different bands of satellite data obtained through remote sensing (Lu et al., 2011; Zelang Miao et al., 2019a; Sishi Wang et al., 2023). Therefore, a model that relies less on a multiple spectral bands would be beneficial for further study.

In recent times, exploring various regression and image classification models has been the key focus of UIS mapping. However, most of these mapping techniques focused on classifying urban land cover rather than specifically addressing UIS mapping (Brodley & Friedl, 1997). Other conventional ways were using binary class (Cheng et al., 2011) or multi-class (Li, 2020) classification methods.

However, employing classification models with binary classifiers encounters significant challenges, particularly when dealing with big data, such as the existence of a substantial class imbalance of an exceptional magnitude. In scenarios where the occurrence of positive class instances is significantly lower than that of negative class instances, the class imbalance poses additional difficulties (Seliya et al., 2021; Shuo Wang & Yao, 2012). Moreover, the disparate prevalence of certain classes adds to the complexity of handling large datasets (Herland et al., 2019).

To address these challenges, the concept of the OCC has been introduced. OCC is a special classification technique that utilizes only one class label for training (Schlachter et al., 2019). This approach tackles various challenges inherent in big data, encompassing significant differences in the availability of classes and the occurrence of highly rare classes (Seliya et al., 2021). Additionally, it enhances data quality through processes like cleaning data, selection of feature, and data downsizing techniques (Seliya et al., 2021). Classifying UIS as a single target (He et al., 2017a) is considered to be one of the recent solutions for UIS mapping.

Conventionally, One-Class classifiers, which concentrate exclusively on a single target class (Deng et al., 2018) has been implemented using machine learning algorithms like Isolation forest (Zelang Miao et al., 2019a), and One-Class Classification through Support Vector Machine (OCSVM) (Dreiseitl et al., 2010; Seliya et al., 2021). However, issues such as the Isolation Forest's limited capability to detect locally clustered anomalies and its extended training time (Liu & Ting, 2012), depicted a room for improvement. Exploring a novel deep learning approach that remains relatively unexplored within the domain of remote sensing may offer promising opportunities for improvement. Additionally, one of the main drawbacks of traditional algorithms is their reliance on a well-defined set of manually crafted features, which often results in neglecting the consideration of spatial information (Liu & Ting, 2012).

Despite the success of conventional machine learning methods in UIS when dealing with a single target class, (Gao & Liu, 2014), there is a lack of accuracy and precision mainly because of neglecting spatial information and due to the limited feature representation. This highlights the necessity for a deep learning architecture. Nevertheless, classifying UIS as a single target class using deep learning remains a challenge. The Deep One-Class Classification framework, recognized as the most recent available technique for OCC, incorporates multiple convolutional layers comprising deep feature learning networks with the combination of a classifier (Lei et al., 2021; Perera & Patel, 2019).

1.4. Research Objectives and Research Questions

The overall objective of this research is to develop a deep learning classification system for UIS mapping using multisource geospatial data. The main objective mentioned previously can be further divided into the following sub-objectives:

1. Identification of suitable freely available geospatial data sources (including remote sensing and VGI) for UIS mapping.
2. Designing a Deep One-Class architecture for UIS mapping.
3. Evaluating the proposed Deep One-class Classification architecture.

To achieve the aforementioned objectives, the following research questions and sub research questions will be addressed:

Research Q1. How can the fusion of multiple geospatial data sources enhance the accuracy of mapping UIS? (Objective 1)

- 1.a Which remote sensing data sources are suitable for mapping UIS and why?
- 1.b What are the VGI data sources selected for mapping UIS?
- 1.c How to use VGI data and remote sensing data sources in an integrated way for accurate UIS mapping?

Research Q2. How can UIS (target class) be classified without taking other land cover classes into account? (Objective 2)

- 2.a How can Deep Learning be used for the One-Class Classification (OCC) approach given UIS as the target class?
- 2.b What is a suitable architecture for one-class classification for mapping UIS?
- 2.c How to prepare dataset for training, validation, and testing?

Research Q3. How can the efficiency of the proposed Deep Learning One-Class Classification architecture be assessed and validated? (Objective 3)

- 3.a How can we consider spatial continuity existence in our dataset in model validation?
- 3.b How can we assess the generalization of the built model?
- 3.c How can we compare the one class and multiclass classification?

1.5. Thesis Structure

This thesis consists of seven main sections and an appendix. The thesis begins with an introduction that elucidates the research problem and the rationale behind the study, and identifies the research gap. This chapter also provides an overview of the thesis, outlining its objectives and research questions. The second division of this thesis presents a comprehensive review of relevant literature, highlighting the existing research conducted in the field. The third section delves into the specific area of study and discusses the datasets employed in this research. The fourth chapter outlines the methods employed to achieve the research goals. In the fifth chapter, the findings and results obtained from the applied methodology are discussed in detail. The sixth chapter concludes the entire research project by summarizing the key findings, identifying any encountered challenges, and proposing potential avenues for future studies. The seventh and final chapter focuses on the ethical considerations associated with this work. Additionally, an appendix is included in this thesis

2. LITERATURE REVIEW

According to (He et al., 2017a; Zelang Miao et al., 2019a), urbanization leads to the escalation of impervious surfaces. (Weng, 2012) states that the necessity of understanding the spatial pattern and distribution of the impervious surface is significant in comprehending urban characteristics. UIS is found to play a significant role in urban-environment relationships. For example, knowledge of impervious surfaces serves as a key parameter for Land Surface Temperature, surface water run-off, urban climate change, and ecological assessment (Alberti, 2005; Alberti et al., 2007; Cadenasso et al., 2007; Gillies et al., 2003; Pauleit et al., 2005). Another notable application of UIS mapping is its relevance in urban planning (Aayog, 2021; Enoguanbhor, 2023; SCHUELER, 1994; Stasolla & Gamba, 2008).

Remote sensing has proven to be a reliable approach for mapping and estimating impervious surfaces. (Weng, 2012) discusses the recent trend of remote sensing emphasizing on different sensors and their spatial resolutions in UIS classification and portrays impervious surfaces as an exceptional case of land cover. UIS classification has been achieved with a wide range of remote sensing data such as LiDAR data (Wu et al., 2019), airborne hyperspectral data (van der Linden & Hostert, 2009), satellite data from optical sensors, SAR (Bai et al., 2019; Sun et al., 2022; Tan et al., 2015; Torres et al., 2012; Y. Wang & Li, 2022; Xiang et al., 2016), and VGI data (Elwood et al., 2012; Zelang Miao et al., 2019b).

(Lu et al., 2014) suggests that remote sensing data with a medium or coarse spatial resolution is most suitable for studying imperviousness in an area. Previous studies focused on mapping impervious surfaces in specific cities by employing multispectral data with a medium spatial resolution as it is crucial for distinguishing impervious surfaces from other land covers (Li, 2020). Furthermore, previous research has proven that high-resolution images with limited spectral bands is inadequate to differentiate urban land covers while hyperspectral images with multiple spectral bands presents the risk of data redundancy (Lu et al., 2014).

According to (Dunkel et al., 2020; Naghavi et al., 2022), VGI data are voluntarily shared open-source data with spatial information. Acquiring VGI data is less time-consuming and cost-effective (McLaren, 2011). Integrating such VGI data with satellite imagery has been an active research in impervious surface studies in urban areas. One such notable work is the integration of OSM, a type of VGI data, with satellite imagery for impervious surface estimation (Fan et al., 2019; Parekh et al., 2021). Another significant research in utilizing VGI data for UIS mapping is by combining social media data with satellite imagery (Z. Miao et al., 2019; Yan et al., 2018).

(He et al., 2017b) executed different One Class Classifier models such as OCSVM, Biased Support Vector Machine (BSVM), Positive-Unlabelled Learning (PUL), Presence and Background Learning (PBL), and Maximum Entropy Model (MAXENT) for the UIS classification. Particularly, the one class classifiers have shown high efficiency in training and good classification accuracies (He et al., 2017b). Moreover, adopting one class classifiers for impervious surface mapping enables addressing the challenges associated with imbalanced datasets and the difficulty in acquiring reference data labels for other classes. These challenges may arise due to limited accessibility to certain land cover types (Fernandez et al., 2011; Z. Xu et al., 2017).

Deep learning, characterized by multiple processing layers, facilitates more efficient feature learning and is appropriate for learning representations of image data (Lecun et al., 2015; Ruff et al., 2018; Schmidhuber, 2015). The selection of appropriate loss functions for feature learning is crucial in the realm of deep learning for one-class classification (Goyal et al., 2020; Lei et al., 2021; Perera & Patel, 2019). The cross-entropy loss function is a notable choice commonly used for multiclass classification tasks (Andreieva & Shvai, 2021). Numerous researchers have made attempts to modify the cross-entropy function for various classification tasks (Kobs et al., n.d.; Mostafa, 2021; Rezaei-dastjerdehei et al., 2020). Similarly, there have been endeavors to employ the cross-entropy loss function with modifications for OCC (Gong et al., 2021; Perera & Patel, 2019). Prominent loss functions utilized for One-Class Classification (OCC) encompass the focal loss function, compactness loss function, bounded loss function, among others (Hong & Member, 2020; Perera & Patel, 2019; Razzak et al., 2020; Wiedemann & Beckmann, 2016). From these options, appropriate loss functions will be chosen for the purpose of this research in order to classify UIS.

Many studies have been conducted on one class classification using deep learning, which is acknowledged to be an up-to-date technique (Ghozatlou et al., 2022; Lei et al., 2021; Ruff et al., 2018). (Lei et al., 2021) presented a DOCC model using convolution layers for satellite imagery, thus demonstrating that DOCC can be adopted for remote sensing data. An additional notable demonstration of DOCC's implementation in the domain of remote sensing is the employment of a specialized deep learning framework tailored explicitly for UAV images (Bah et al., 2019).

3. STUDY AREA AND DATASET

3.1. Selected study Area

The western region of the Netherlands has been selected as the testing area for this classification approach due to the ample availability of updated datasets encompassing both satellite imagery and VGI. Moreover, urbanization in the Netherlands is a significance phenomenon as the population residing within its urban areas is witnessing notable growth. This trend can be attributed to the emergence of new employment opportunities in the job market (Beckers & Boschman, 2019; Hans & Koster, 2018). This process of urbanization in the Netherlands has led to a substantial increase in the extent of impervious surfaces (Costa et al., 2021). Therefore, selecting the cities in the Netherlands as our case study provides a promising opportunity to implement our methodology and achieve accurate mapping of UIS.

For this research, as mentioned earlier, the urban extent of the Netherlands is chosen in such a way that more emphasis is given to the urbanized cities of the country, which are housed in the western region. These cities are Amsterdam, the Hague, Utrecht, Rotterdam, and some extents of Arnhem. The geographical coordinates for the study area extent are as follows; minimum longitude- $4^{\circ} 11' 12.7998''$ E, maximum longitude- $6^{\circ} 19' 20.2722''$ E, minimum latitude- $51^{\circ} 39' 54.579''$ N, and maximum latitude- $52^{\circ} 36' 52.776''$ N. Figure 1 represents the chosen extent for this study.

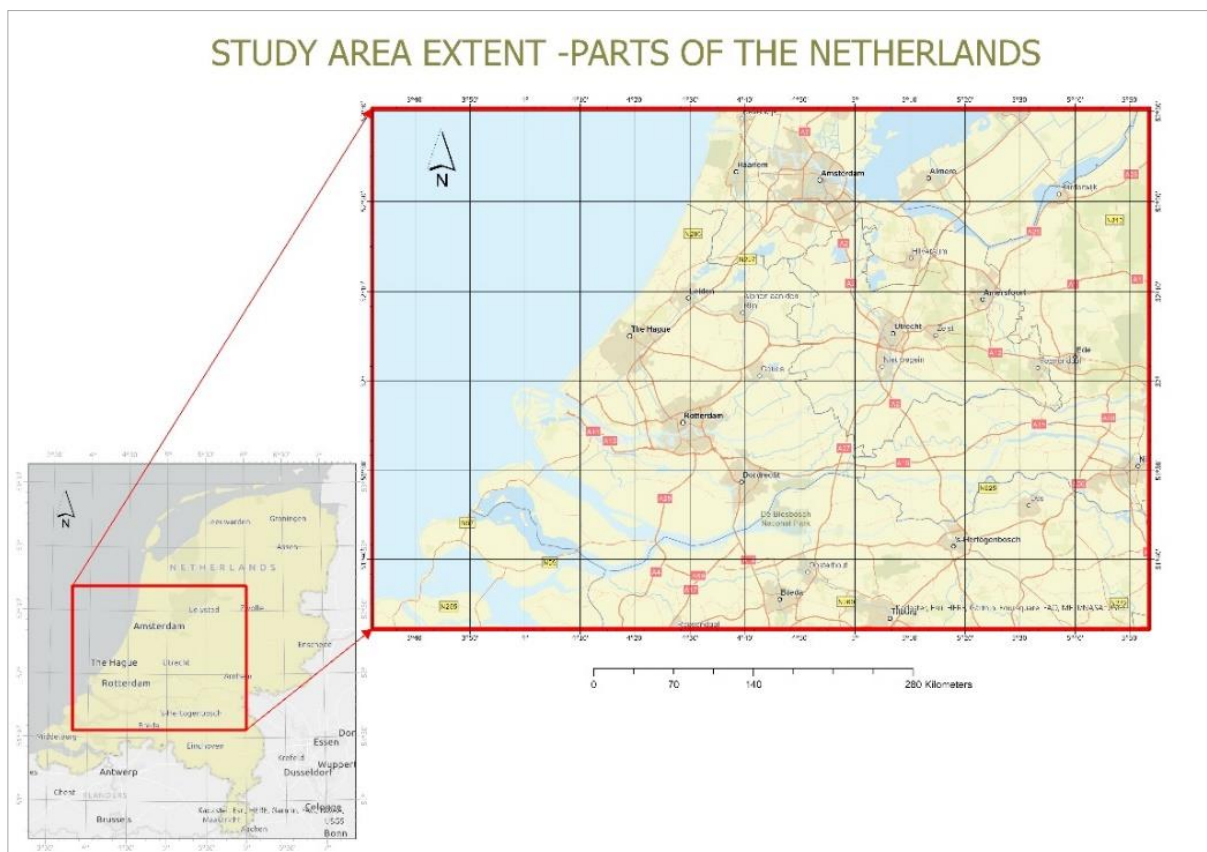


Figure 1 Study Area Map

3.2. Datasets considered for the study

Sentinel-2, an Earth observation mission that was developed by the European Space Agency (ESA), facilitates global monitoring, including land cover change mapping with its high-resolution imaging capability (Drusch et al., 2012). Sentinel-2 comprises twin satellites, namely Sentinel-2A and Sentinel-2B, which were set in motion in June 2015 and March 2017, respectively (Main-Knorn et al., 2017). The Sentinel-2 Multispectral Imager (MSI) records imagery data in 13 spectral bands spanning the shortwave infrared, near-infrared (NIR), and visible segments of the electromagnetic spectrum (Gašparović et al., 2018). These satellites provide frequent revisits to the same region every 5 days, enabling the collection of multispectral imagery at a fine spatial resolution. This satellite mission is well-suited for capturing information about impervious surfaces (Misra et al., 2020).

In a prior research, it was demonstrated that the impervious surface map generated from Sentinel-2A data at a 10-meter resolution contained more detailed information compared to the impervious surface map derived from Landsat 8 OLI imagery at a 30-meter resolution (R. Xu et al., 2018). Furthermore, the Sentinel-2A impervious surface map from the same study effectively depicted continuous roads and accurately delineated building boundaries, whereas the Landsat 8 OLI image struggled to differentiate these boundaries (R. Xu et al., 2018).

VGI is considered to be a potential source for understanding the surface of the Earth (Goodchild, 2007). OSM is a freely available and open geospatial dataset that represents various features present on the Earth's surface like buildings, roads, etc. (Fitri et al., 2022). Among VGI datasets, OSM holds a significant value for the GIS and remote sensing community offering a freely accessible and editable database along with a comprehensive map of the world contributed by volunteer mappers (Grinberger et al., 2022). Previous researches utilized OSM data specifically roads, buildings, pavements, and bridges, to identify impervious surfaces (Fan et al., 2019; Mao et al., 2022; Parekh et al., 2021). Furthermore, studies have demonstrated the integration of remote sensing data and OSM data for studying impervious surfaces to be effective (Fan et al., 2019; Mao et al., 2022; Parekh et al., 2021).

Additionally, Twitter represents another valuable and state-of-art source of VGI. The geotagged nature of Twitter data provides a spatial component, making it an effective tool for gathering location-based information (Elwood et al., 2012). When combined with remote sensing data, Twitter has proven to be a useful spatial data source for multiple applications (Cervone et al., 2016; Devkota et al., 2019; Schnebele et al., 2014; Shao et al., 2021).

An interesting study on Twitter's role in understanding human mobility within urban dynamics demonstrated that topic-related tweets can serve as a potential proxy for real-world activities in urban spaces like workplaces and residential spaces. This correlation was further validated by comparing tweet-derived data with work and residential population statistics from census records (Steiger et al., 2015). This implies that using geotagged tweets can serve as a viable alternative for capturing the spatial distribution of urban inhabitants, which correlates indirectly with UIS. Additionally, several studies have extensively examined the association between Twitter usage and urban land use. These investigations aim to characterize urban land use by analysing the activities of Twitter users (Frias-Martinez & Frias-Martinez, 2014; Z. Miao et al., 2019; Soliman et al., 2017).

The purpose of this study is to examine the open geospatial data resources that are currently available to enhance the accuracy of mapping UIS. For 2022, optical data obtained from Sentinel-2 imagery was chosen, with a specific focus on the essential bands: blue, green, and red (refer to table 1). These bands were chosen

to assess the effectiveness of a deep learning feature extractor. The data was chosen based on its high spatial resolution of 10 meters, making it suitable for detailed analysis. Furthermore, its cost efficiency and compatibility with recent techniques were considered as advantageous factors in the selection process.

Name	Wavelength	Description
B2	496.6 nm	Blue
B3	560nm	Green
B4	664.5nm	Red

Table 1 Spectral bands of Sentinel 2 utilized for this study

Additionally, as a supportive data source, the VGI data sources OSM and Twitter were employed for the suggested UIS mapping method. For this research, only the building and road features from the OSM dataset was considered. These features are chosen due to their demonstrated high reliability in accurately representing impervious surfaces (Parekh et al., 2021). Moreover, the geographical location of tweets is utilized while neglecting sensitive details like user identity, textual content, and any attached multimedia. The distribution of Twitter data used for this study is depicted in Figure 2.

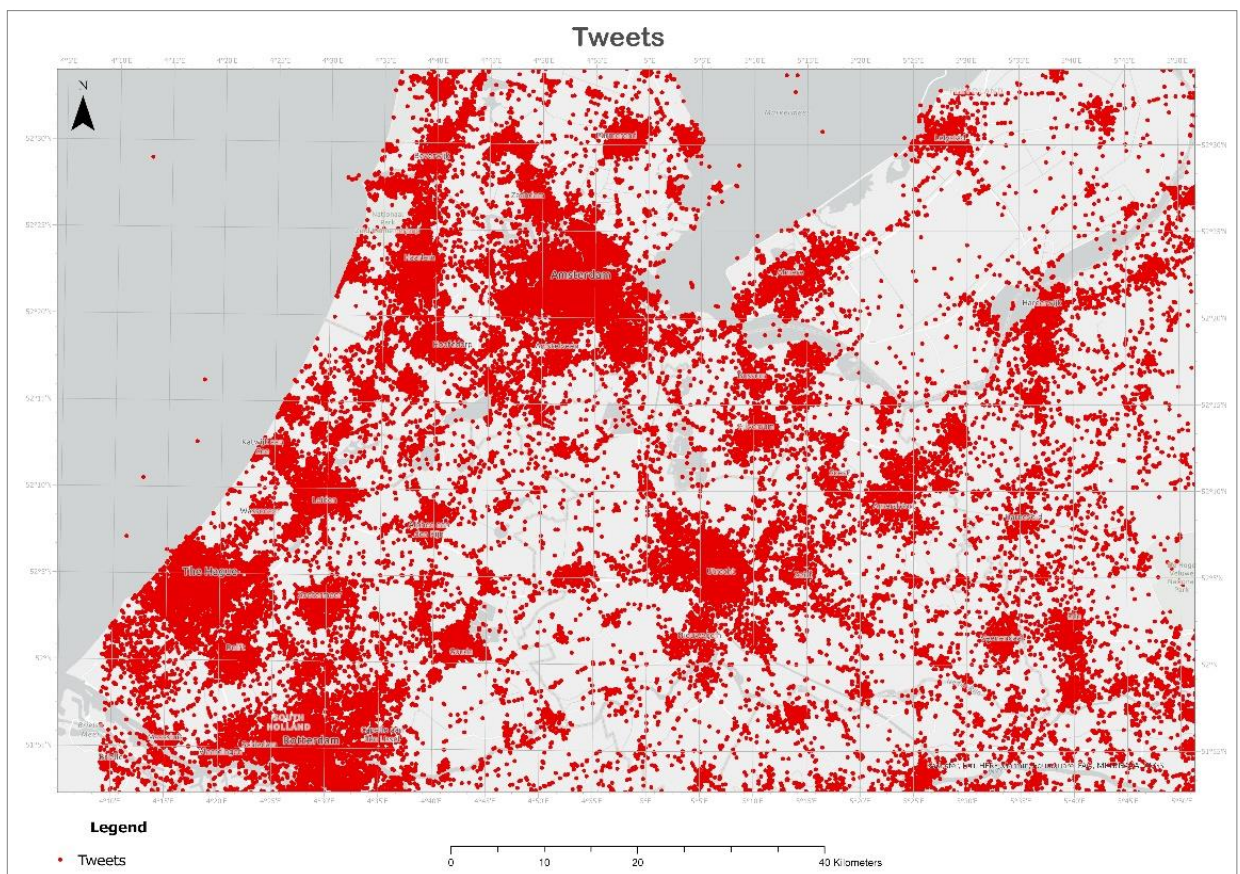


Figure 2 Map depicting the geographical locations of user tweets.

4. METHODOLOGY

4.1. Acquiring Quality data

There have been several attempts to extract impervious surfaces using machine learning algorithms and object-oriented segmentation methods, typically relying on the spectral features of the satellite imagery (Fan et al., 2019; F. Huang et al., 2019; Mao et al., 2022). However, in this research work, a new approach is introduced for the extraction of UIS patches. Unlike traditional methods that rely solely on spectral features derived from satellite imagery, this approach incorporates the association of satellite imagery with VGI data, specifically Twitter and OSM data. By integrating these additional data sources, a rule-based approach is employed to extract UIS patches, providing a new perspective. This proposed methodology not only enhances the extraction process but also enables the creation of reliable labeled datasets of satellite imagery patches depicting UIS by considering tweet locations and OSM as references.

Twitter is commonly utilized by individuals in proximity to human-made structures such as buildings, roads, and various concrete surfaces, collectively referred to as impervious surfaces (Z. Miao et al., 2019; Steiger et al., 2015). The study hence relies on the fact that the tweets originate from places that are in close proximity to urban structures which in turn can be related to impervious surfaces.

The tweets from the western extent of the Netherlands were provided by the Faculty of Geo-Information Science and Earth Observation of the University of Twente. These tweets are in CSV format and include latitude and longitude information. Observations in the CSV that lacked the latitude and longitude information were excluded from the dataset. The initial filtering process involved removing tweets located in vegetation areas and water bodies. To accomplish this, the tweets were converted to shapefiles with the Coordinate Reference System (CRS) of EPSG 28992. Land cover data in the form of polygon shapefiles obtained from pdok were utilized to remove tweets associated with water bodies and parks. Geopandas¹ overlay function, specifically employing the "contains" option, facilitated this removal process. The selected tweets were subsequently stored in CSV format for further processing. Figure 3 depicts the flowchart detailing the aforementioned process, while Figure 4 presents the map illustrating the distribution of tweets across vegetation and water areas.

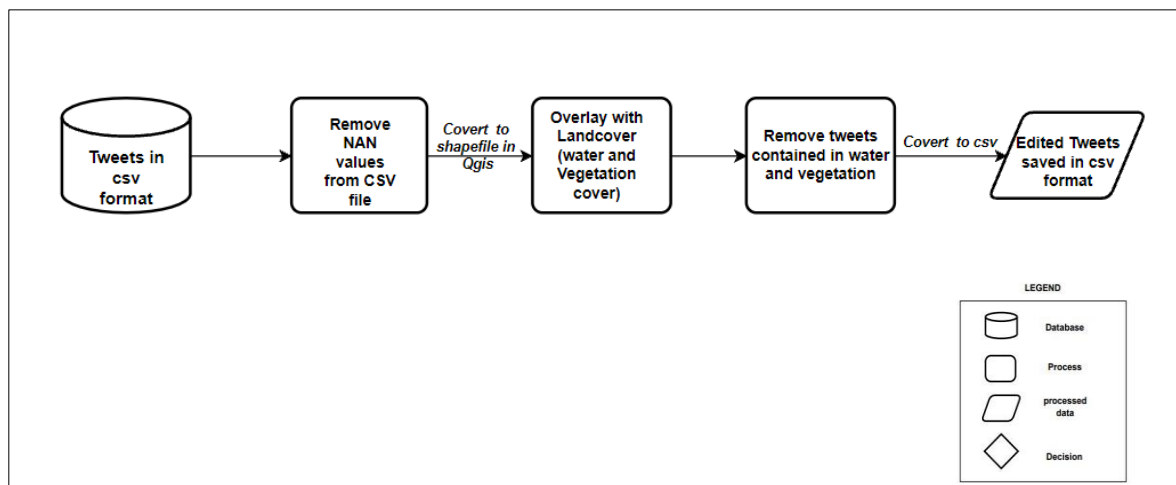


Figure 3 Flowchart representing the methodology of pre-processing.

¹ <https://geopandas.org/>

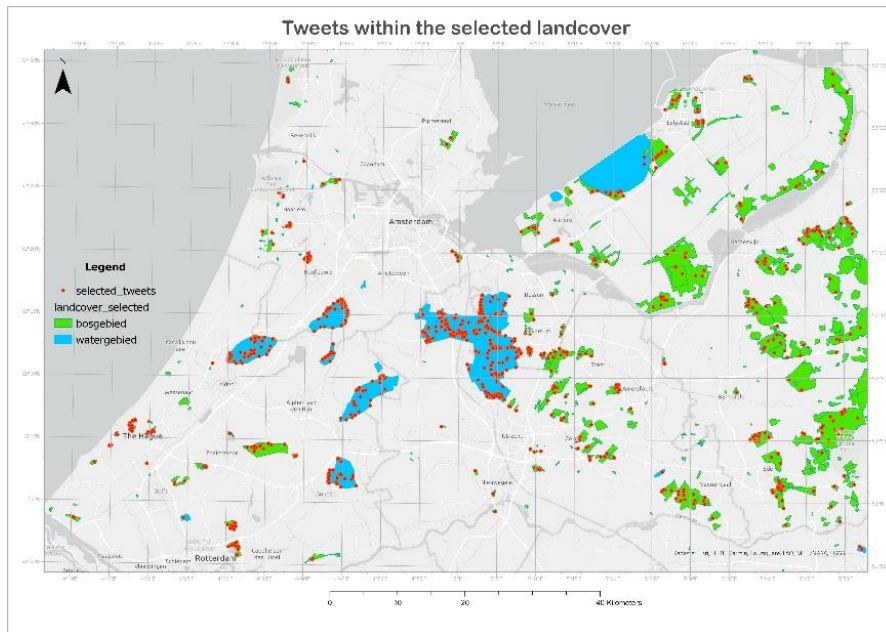


Figure 4 Tweets within the waterbodies and forest areas

To identify more reliable data for detecting impervious surfaces, several pre-processing steps were performed using the pandas² and geopandas³ libraries. Initially, a "count" column was added to the geodataframe, indicating the number of tweets recorded at each location. This count was computed for each tweet and added as a new column in the data frame, representing the intensity or frequency of tweet occurrences at specific locations. Subsequently, a buffer of approximately 500 meters was created around each Twitter point using the geometry.buffer⁴ function from the geopandas package. This buffer size was chosen based on trial and error basis as 500 meters promises to give a wide spread out tweet points. The number of tweets within these buffers was then calculated and updated in the dataframe as the "buffer_counts" column.

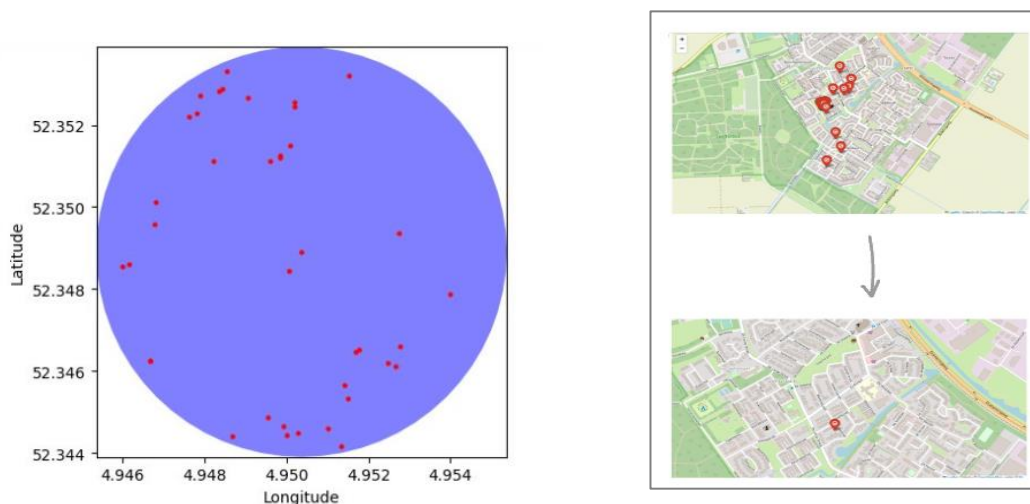


Figure 5 A buffer created around one of the selected tweets (left) and the tweet reduction after selection process (right)

² <https://pandas.pydata.org/docs/>

³ https://geopandas.org/en/stable/docs/advanced_guide.html

⁴ https://geopandas.org/en/stable/docs/user_guide/geometric_manipulations.html

Based on the created columns, two conditions were applied to identify Twitter points with a high probability of representing impervious surfaces. The first condition required the intensity (count) to be higher than the 25th percentile of the count values, which was determined through trial and error. Similarly, the second the condition required the buffer count to be greater than the 25th percentile of the buffer counts. Twitter points that satisfied both conditions were selected, as they possess the highest probability of being impervious and are well-distributed. This shows that the tweets which are selected have a higher intensity of tweet occurrences.

Some towns or cities had a low number of tweets, while others had dense clusters of tweets. To address this imbalance, tweet points in cities with dense clusters were selectively removed. Also, to ensure that the acquiring impervious labels is representative and not biased towards similar structures, it was necessary to distribute the tweets across the entire study area. This included assigning a new buffer with a radius of 10,000 meters to each tweet, considering the distances between cities in the Netherlands. Tweets that were in close proximity within these buffers were then removed. These steps helped to remove points that were in close proximity and belonged to the same structure. Also, it helped to create a more balanced and representative dataset for further analysis.

After selecting the tweets, a bounding box of size 64x64 pixels was created around each selected tweet as the centre point. The OSM data, which encompasses elements such as houses and roads that possess impervious characteristics (Fan et al., 2019; Perekh et al., 2021), was integrated to obtain reliable data. The number of roads and buildings within the extent of each bounding box was counted using the osmextract⁵ package. To ensure the selection of high-quality data, only bounding boxes with counts of buildings and roads above the 25th percentile were considered. The selected bounding boxes were used to extract Sentinel-2 imagery from Google Earth Engine. The imagery extraction process specifically targeted scenes with a maximum of 10% cloud coverage within the bounds. This approach guarantees the extraction of patches that are considered to be impervious surfaces in urban areas. These acquired patches (refer to figure 8) are used for detecting UIS using a deep one-class classification model.

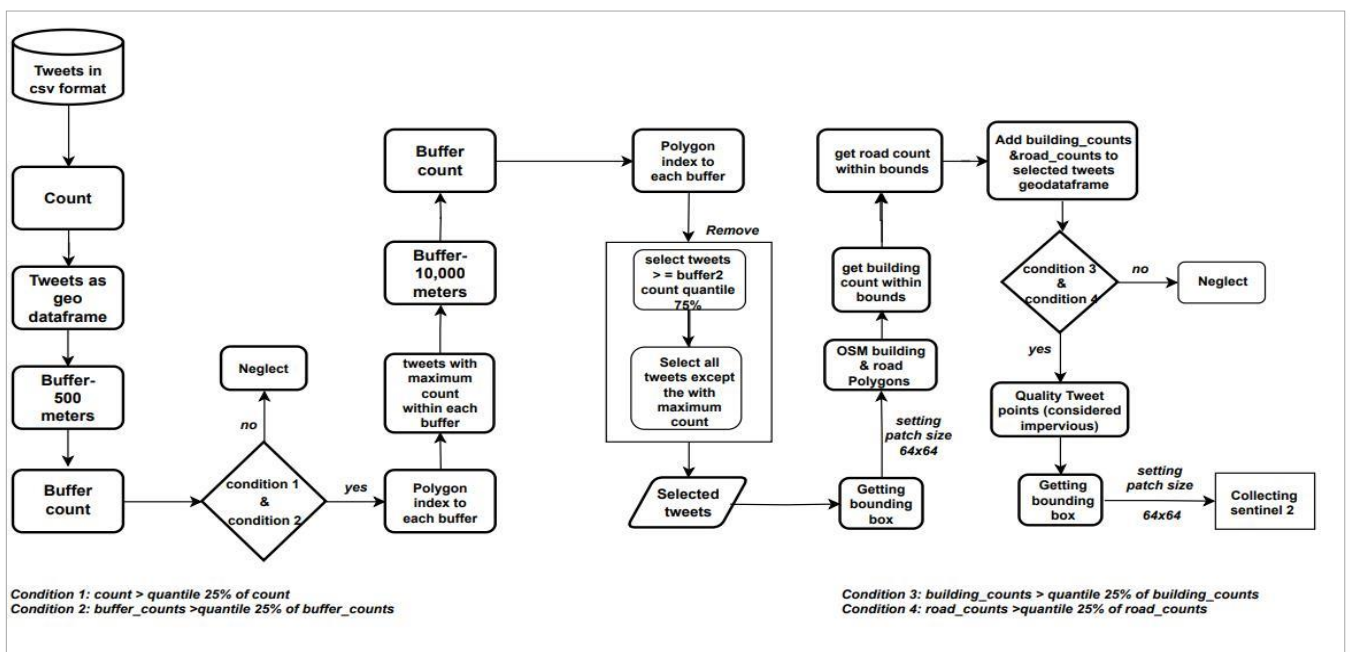


Figure 6 Flowchart representing the methodology of this study.

⁵ <https://pypi.org/project/osmextract/>

Figure 6 illustrates the flowchart outlining the methodology for obtaining the desired satellite dataset. Figure 7 displays the map showcasing the selected tweet's locations, which serve as the center points for acquiring the satellite patches using the aforementioned methodology. Totally 1659 patches were collected.

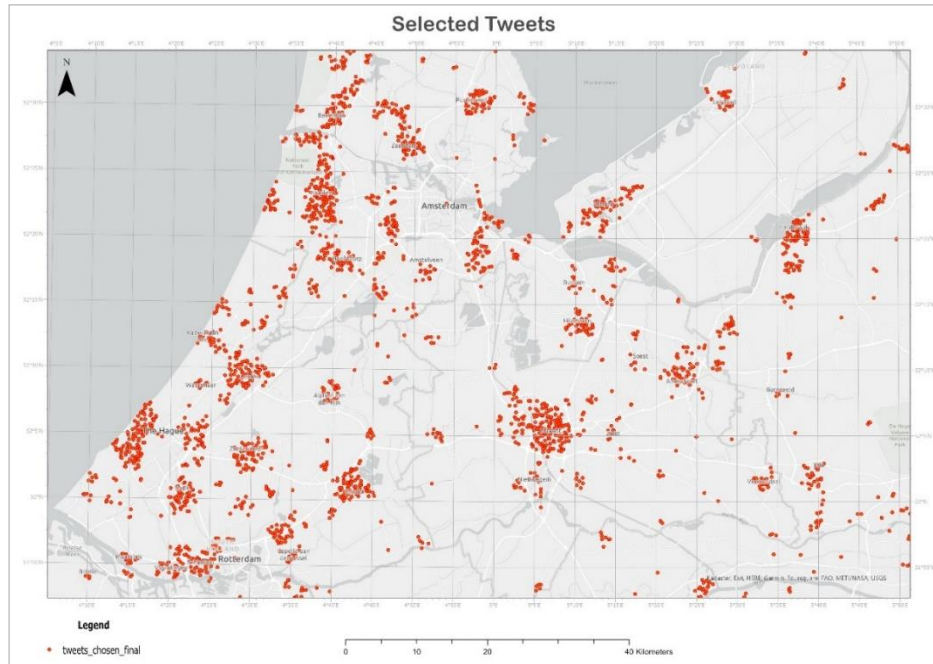


Figure 7 Map of selected tweets after pre-processing

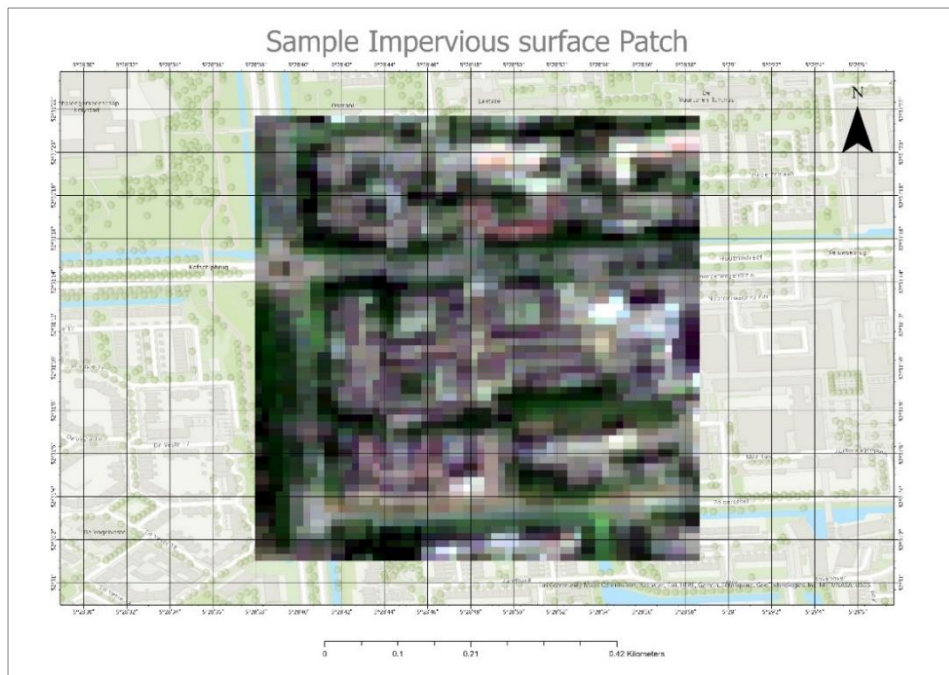


Figure 8 Sample patch acquired through the proposed pipeline

4.2. Deep learning model for Impervious surface detection and mapping

4.2.1 Deep One-class Classification

As discussed previously, the most advanced approach currently employed to address OCC problems is through the utilization of deep learning techniques. UIS mapping can be conceptualized as an OCC problem, with the impervious surface serving as the target or positive class. In this study, the CNN, a widely recognized deep learning model, will be employed to construct the Deep One-Class Classification (DOCC).

Input data and data preparation: The DOCC comprises two parallel pre-trained CNN networks. Each network requires two distinct sets of data: the target dataset, which contains the class that needs to be detected, and the reference dataset, which consists of a mixture of other data that is irrelevant to the target class (specifically, any surface other than the impervious class).

Thus here, the previously extracted patches of impervious surfaces from the proposed pipeline is taken as the target class. These target dataset is of size 64x64. The reference dataset, on the other hand, is based on the EuroSAT dataset, which utilizes sentinel 2 satellite imagery (Helber et al., 2019). The patches in the reference dataset are also of same size as the target dataset and consist of a combination of RGB spectral bands from various classes, excluding the impervious surface. However, the reference dataset is not labelled.

Therefore, the target dataset consists of 1659 images from previously proposed method, while the reference dataset comprises 19,000 EuroSAT images from various classes in total. The target and the reference datasets are divided into training and test sets using a test size of 30%. The number of datasets used as training and testing in this research are presented in Table 2. Figure 9 provides an illustration of the shape of the training and testing datasets.

Reference training data	13300 images
Target training data	1161 images
Reference testing data	5700 images
Target testing data	498 images

Table 2 Reference and Target Dataset split

```
print(Rdata_test.shape)
print(Tdata_test.shape)

(5700, 224, 224, 3)
(498, 224, 224, 3)

print(Rdata_train.shape)
print(Tdata_train.shape)

(13300, 224, 224, 3)
(1161, 224, 224, 3)
```

Figure 9 Code snippet of the shape of training and testing datasets

Before feeding the dataset into the initial pre-trained convolutional network, it is necessary to reshape the dataset to match the desired input patch size of $h \times w \times c$ (Lei et al., 2021). Here, the variable h represents the height of the image, w represents the width of the image, and c indicates the number of spectral bands

considered (Lei et al., 2021). In this research, the DOCC is initially showcased using three bands (RGB) with an input shape of (224, 224, 3), based on the VGG16 pre-trained model. A limited number of bands are employed to demonstrate the efficacy of deep feature learning in UIS classification.

Loss Functions: The Positive and Unlabelled Learning (PUL) framework is employed, where the impervious surface dataset is considered as the Positive labels. PUL aims to identify an appropriate classifier based on the available positive and unlabelled data (Gong et al., 2021). The PUL approach assumes that the unlabelled dataset has the potential to belong to either the positive class or the negative class (Bekker & Davis, 2020; Gong et al., 2021; He et al., 2017a). To achieve this two major loss functions are introduced by (Perera & Patel, 2019) namely, Compactness loss and Descriptiveness loss. The compactness loss evaluates the similarity within the data belonging to the same class by estimating the intra-class variance of the target class. This estimation is accomplished using the Euclidean distance metric. On the other hand, the descriptiveness loss measures the ability to learn features that can effectively distinguish the target dataset from the reference dataset, employing the cross-entropy method (Perera & Patel, 2019). Later these two losses are combined to acquire the total loss.

The formula for the compactness loss (l_c) (Perera & Patel, 2019) is given by,

$$l_c = \frac{1}{n} \sum_{i=1}^n z_i^T z_i$$

Here z denotes the distance of the given sample from the mean of rest of the samples. Also, the variable n corresponds to the amount of samples.

The categorical cross-entropy in Keras, along with the Softmax function, is applied to the reference dataset to compute the loss of descriptiveness (l_d). The general formula for the cross entropy (Chaithanya et al., 2021) is given by,

$$L_{ce} = - \sum_{i=1}^n t_i \log P_i$$

Thus the calculation of l_d is derived using the above base entropy formula, denoted as L_{ce} , which employs true(t_i) labels and predicted(P_i) labels.

The total loss (l_t), which is framed with reference to (Perera & Patel, 2019), is computed by combining the compactness and descriptive losses in the following formula,

$$l_t = l_d + w l_c$$

Here, 'w' represents compactness weight which is given on trial and error basis.

DOCC Architecture: The DOCC architecture is based on two important parameters: a deep learning feature extractor and a classifier (Bah et al., 2019; Perera & Patel, 2019). The deep feature extractor is constructed with parallel CNN architecture (Perera & Patel, 2019). Two pre-trained VGG 16 CNN model are employed to extract deep features, but with a modified approach. Two models, namely the target network and reference network, are constructed using the said pre-trained CNN. The target network is

trained using the image patches from impervious surface dataset (target) while the reference network is trained with the image batches from EuroSAT dataset.

Training phase: The target network and the reference network in this study consist of a series of continuous convolution, pooling, and normalization layers (refer to figure 10) which are executed using keras⁶ and tensorflow⁷ packages. These networks are initialized in parallel, with each network utilizing its respective input dataset. The target network computes the compactness loss within the impervious surface dataset by estimating the intra-class variance. Conversely, the reference network estimates the descriptiveness loss using the EuroSAT dataset. These two losses mark the completion of the forward pass. The total loss is then calculated by applying the previously mentioned formula, with a weight of 8 assigned to the compactness loss. The weight w is adjusted in a way that the descriptiveness of the learned features is of comparable importance to that of compactness loss. The training process continues until the total loss reaches a point of convergence, indicating that the network has achieved stability. Later, fine-tuning of these networks are performed by changing hyperparameters like epochs and batch size.

Layer (type)	Output Shape	Param #
input_1 (InputLayer)	[(None, 224, 224, 3)]	0
block1_conv1 (Conv2D)	(None, 224, 224, 64)	1792
block1_conv2 (Conv2D)	(None, 224, 224, 64)	36928
block1_pool (MaxPooling2D)	(None, 112, 112, 64)	0
block2_conv1 (Conv2D)	(None, 112, 112, 128)	73856
block2_conv2 (Conv2D)	(None, 112, 112, 128)	147584
block2_pool (MaxPooling2D)	(None, 56, 56, 128)	0
block3_conv1 (Conv2D)	(None, 56, 56, 256)	295168
block3_conv2 (Conv2D)	(None, 56, 56, 256)	590880
block3_conv3 (Conv2D)	(None, 56, 56, 256)	590880
block3_pool (MaxPooling2D)	(None, 28, 28, 256)	0
block4_conv1 (Conv2D)	(None, 28, 28, 512)	1180160
block4_conv2 (Conv2D)	(None, 28, 28, 512)	2359808
block4_conv3 (Conv2D)	(None, 28, 28, 512)	2359808
block4_pool (MaxPooling2D)	(None, 14, 14, 512)	0
block5_conv1 (Conv2D)	(None, 14, 14, 512)	2359808
block5_conv2 (Conv2D)	(None, 14, 14, 512)	2359808
block5_conv3 (Conv2D)	(None, 14, 14, 512)	2359808
block5_pool (MaxPooling2D)	(None, 7, 7, 512)	0
flatten (Flatten)	(None, 25088)	0
dense (Dense)	(None, 1000)	25089000
re_lu (ReLU)	(None, 1000)	0
dropout (Dropout)	(None, 1000)	0
dense_1 (Dense)	(None, 1000)	1001000
re_lu_1 (ReLU)	(None, 1000)	0
dropout_1 (Dropout)	(None, 1000)	0
dense_2 (Dense)	(None, 1000)	1001000
dense_3 (Dense)	(None, 7)	7007
=====		
Total params: 41,812,695		
Trainable params: 27,098,007		
Non-trainable params: 14,714,688		

⁶ <https://keras.io/>

⁷ <https://www.tensorflow.org/>

**Figure 10 Summary of the Model architecture
(Target and Reference model)**

In this way, the deep features are learned for One-Class Classification. The flowchart of the training phase is represented in the figure 11 below.

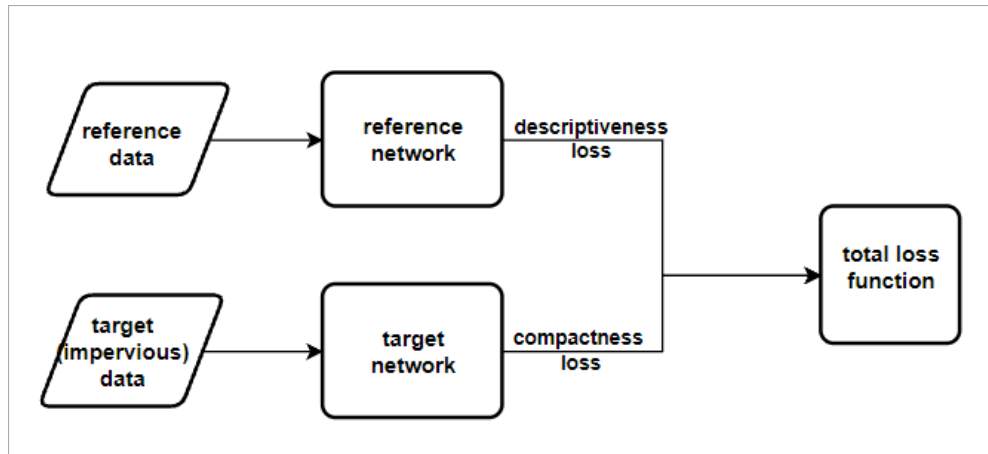


Figure 11 Workflow of training phase

Testing phase: In the testing phase, there are two important stages; template matching and classification. In the template matching stage, a subset of the impervious dataset is taken and by employing the target network, which has the weights learned during the training stage, a set of features are extracted.

Test images are a combination of both the reference dataset and the impervious surfaces are given as new input samples. Using the trained target network as a feature extractor, features are generated from a test images as well. Subsequently, the features obtained from both the network, namely the target dataset and the testing set, are compared using an appropriate classifier. This classifier is constructed using the K-Nearest Neighbour algorithm with a simple Euclidean distance as the matching function. The purpose of this classifier is to determine whether the test sample belongs to an impervious surface or not. The Euclidean distance, which serves as a straightforward matching function, is employed. The matching scores (s) derived from the classifier are used to identify and detect the impervious targets.

Class = 0, if $s > k$
 Class = 1, if $s \leq k$,

In the above equation, the value of k represents the threshold used to determine whether the test image belongs to class 0 or class 1. The selection of the k threshold is done through an iterative process of trial and error, considering the model's performance metrics. If the matching score(s) surpasses the threshold value of k, the sample is classified as Class 1, representing the target class, which in this case corresponds to impervious surfaces. On the other hand, if the matching score(s) falls below the threshold, the sample is classified as Class 0, indicating other surfaces. The figure 12 shows the testing phase stages.

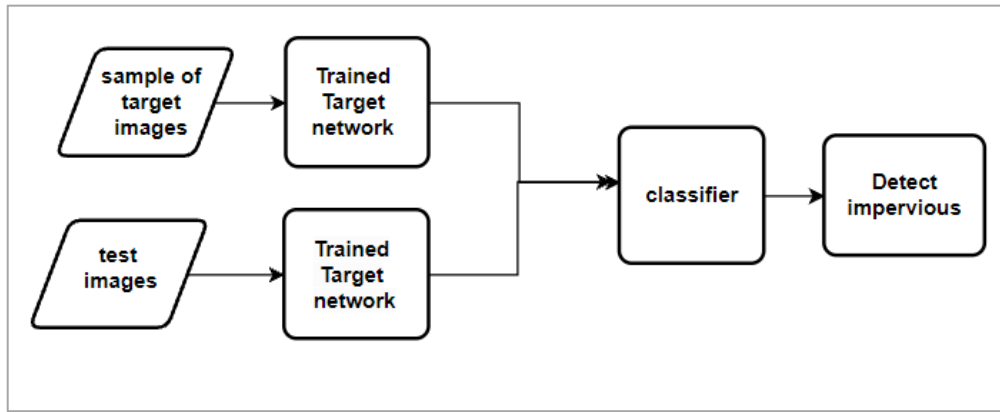


Figure 12 Workflow of testing Phase

Evaluation: Previous research has utilized evaluation metrics such as precision, recall, F1 score, and confusion matrix for evaluating the classification models (Devkota et al., 2019; Lei et al., 2021; Zhao et al., 2022). Therefore, these metrics are utilized to assess the performance of the proposed DOCC model.

A confusion matrix is a common quantitative technique that provides knowledge on the output predictions of a classification algorithm (Strobel et al., 2018). This gives the information about the true positives, false positives, true negatives, and false negative of the classification model output. Recall is a metric that measures the ratio of correctly predicted real positive instances to the total number of actual positive instances (Powers, 2020). Precision, on the other hand, is a metric that quantifies the proportion of predicted positive instances that are indeed real positives (Powers, 2020). The combination of these two metrics gives the F_1 score (Zhao et al., 2022),

$$F_1 \text{ score} = 2 \times \frac{\text{Precision} \times \text{Recall}}{\text{Precision} + \text{Recall}}$$

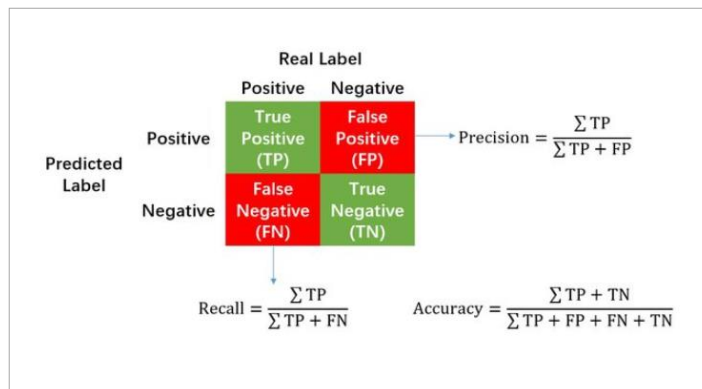


Figure 13 Representation and formula for the evaluation metrics (Ma et al., 2019)

Figure 13 gives the formula and representation of the evaluation metrics discussed.

4.2.2 Deep Multi-class Classification

A multi-class classifier is executed to compare the previously employed one-class classifier with a multi-class classifier. The purpose of multi-class classification is to classify the given dataset into multiple classes (Jha et al., 2019). Thus, a multi-class classifier, unlike the one-class classifier, requires labelled data for each of the classes.

Input dataset and data preparation: The data utilized for this study consists of patches specifically generated for this research that are combined with land cover classes obtained from the publicly available EuroSAT dataset. The land cover classes utilized in this multiclass classification model include Forest, Herbaceous Vegetation, Permanent Crop, Annual Crop, River, SeaLake, Pasture, and Impervious Surface. Only RGB channels of the images are utilized in this analysis. Here the dataset with multiple land cover labels is split into test and train with test size of 30%.

Multiclass classification architecture: The CNN architecture is utilized to execute the multi-class classification and it is executed similar to the DOCC but trained with CNN network for multiclass classifier. The forward function applies the layers of the CNN sequentially to the input in the specified order.

Training and Testing: During the stage of training, the model iterates several steps including forward propagation, loss computation, and backpropagation, on the training data. The cross-entropy loss function effectively discerns the distinctions between the features of each class. Subsequently, during the testing phase, the model is evaluated using the test dataset to assess its performance. This facilitates a precise assessment of the model's performance and capabilities.

Evaluation: The deep learning multi-class model is evaluated using the same set of evaluation metrics as the DOCC. The F1 score, precision, recall, and confusion matrix are among these measures. This enables a comprehensive comparison between the performance of the multi-class classifier and the DOCC. By comparing the results, we gain insights into the effectiveness of the one-class classifier in comparison to the multi-class classifier.

4.2.3 Comparison with the existing Global Impervious Map

A window with the dimension of the selected patches was set up that is 64 x 64, and a stride of 2 pixels was chosen to determine the moving window's step size. This window was then moved across the input Sentinel-2 imagery and extract patches centred at each pixel location. These patches were run on the model thus enabling us to compute an impervious classification on a pixel-wise basis. Subsequently, we compared this generated UIS map with the GISA map for evaluation.

The Global Impervious Surface Area (GISA) map, utilizing a combination of Sentinel 1 and Sentinel 2 imagery, provides valuable information spanning from 1972 to 2019 and it is notable for being the first map with a 10-meter resolution that is globally available (X. Huang et al., 2022). In addition, the GISA map is known to offer improved accuracy compared to that of previously existing maps. Therefore, conducting a comparative analysis between our UIS map and the GISA map holds substantial value.

5. RESULTS AND DISCUSSIONS

5.1 Results and dicussion on Deep One-Class Classification (DOCC)

Initially, when the dataset was subjected to DOCC, the obtained results were unsatisfactory. Therefore, some modifications on the weight of the loss function and hyper parameters were made during the feature learning phase. The training process involved the computation of the total loss function using both the target and reference models. The graph depicting the initial loss versus epoch is presented in figure 14. It shows the descriptiveness loss and total loss overlap. A negligible compactness loss can be seen when a compactness weight 'w' value of 0.5 is assigned in the equation $l_t = l_d + wl_c$. This indicates a need for adjustments in the computation of the total loss function.

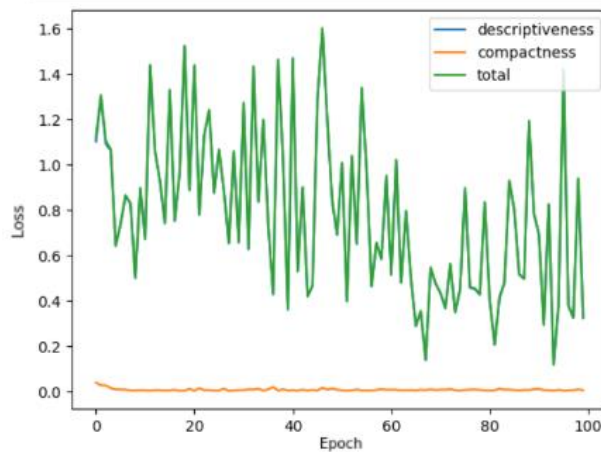


Figure 14 Graph showing initial loss versus epoch

According to (Perera & Patel, 2019), the value of the should be chosen carefully while considering extremes of zero or a large number as these can result in uninformative outcomes. Additionally, when dealing with one-class problems, it is advisable to assign greater weightage to the loss of the reference network, specifically the descriptive loss (Perera & Patel, 2019). Considering this, the weight was determined within a reasonable range through a trial-and-error process. The analysis revealed a significant disparity was observed in the loss function graph. As a result, the model has been adjusted to assign nearly equal importance to both the descriptiveness loss and comparative loss. The new graph is represented in figure 15 where one can note that the total loss considers both the losses but with slightly higher preference to descriptiveness loss.

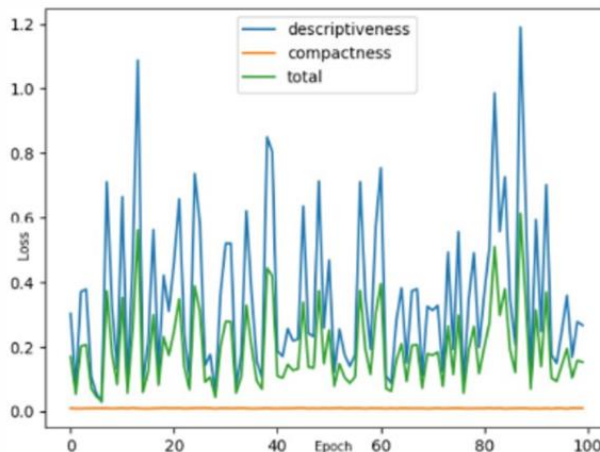


Figure 15 Graph showing loss versus epoch after changes in loss function

Hyperparameters tuning:

The DOCC method employs a combination of CNN networks, as mentioned previously. The CNN block consists of several layers, notably the initial layer with a linear activation function, which performs linear input transformations. This is followed by a ReLU activation function layer. To prevent overfitting, a dropout regularization technique is applied with a dropout rate of 0.3, meaning that 30% of the units are randomly dropped out during training. This dropout rate is selected to strike a balance as a higher value can lead to under learning, while a lower value may have a negligible effect.

The learning rate was identified as a significant parameter with a crucial impact. When the learning rate was set to 0.001, along with 100 epochs and a batch size of 10, the results depicted in Figure 15 were obtained. However, by adjusting the learning rate to 0.00001 based on the study by (Perera & Patel, 2019), noticeable improvements were observed in the curve patterns of the graph. To further enhance training and promote the model's generalization and performance, modifications were made to the epoch and batch size, which were adjusted to 60 and 16, respectively. Additionally, regularization techniques such as dropout with a rate of 0.2 and batch normalization were introduced. The effects of these alterations are demonstrated in Figure 16, which exhibits a significant decrease in the losses during training, indicating enhanced performance.

Scientifically, it is commonly understood that decreasing the learning rate can yield better results when combined with an increased number of epochs. However, in this specific scenario, the relationship is not linear due to the simultaneous adjustment of the batch size. Based on the observations from Figure 16, it can be inferred that after epoch 50, there is no substantial decrease in the loss.

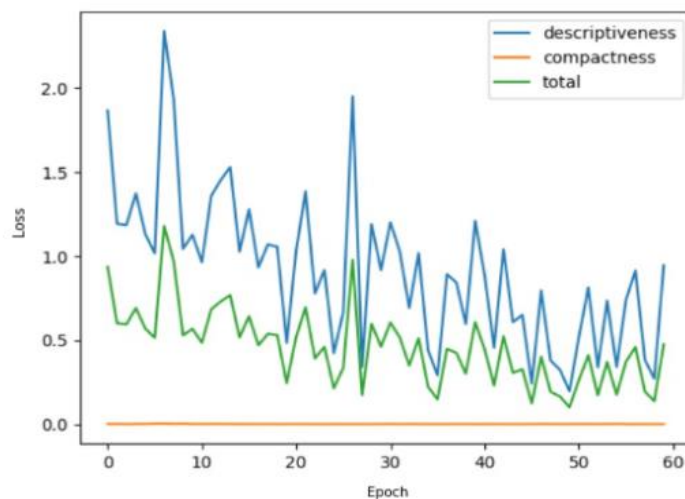


Figure 16 Graph showing loss versus epoch after hyperparameter tuning

Classification evaluation: During the classification process, the testing phase of the deep learning model involved utilizing the test data from both the target and reference datasets. To detect whether the surfaces were impervious or not, the datasets from the target and class and the other reference classes with equal split of 6198 images out of which 498 images were impervious and the remaining were pervious. These images were combined and shuffled for testing. This combined dataset was then fed into the model for prediction and classification. The figure17 shows the predicted scores versus the true label graph, here the

predicted scores represent the likelihood of the instances belonging to a particular class. Here the 1 represents the target class and the 0 represents the reference class. This is to show the separability of the classes. There is a minimal overlap showing an effective separability.

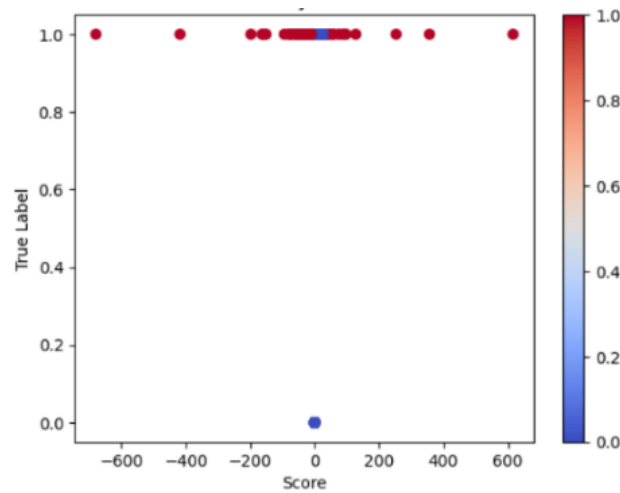


Figure 17 Graph depicting predicted scored versus true labels

The model demonstrated a high accuracy of around 98% (0.977896). The efficiency of the model is further revealed through the analysis of the confusion matrix (refer to figure 18), which indicates a minimal number of incorrectly detected images. The figure 19 depicts the sample images which are predicted as true positives, true negatives, false negatives and false positives. Additionally, the precision and recall metrics were found to be approximately 97% and 74% respectively, indicating the model's strong ability and reliability in predicting positive instances.

In classification models, the F1 score is often prioritized over individual scores. In this case, the F1 score, which considers both precision and recall, is calculated to be approximately 0.844. This value, close to 1, indicates that the model performs well in minimizing both false positives and false negatives. The F1 score serves as a comprehensive evaluation metric, reflecting the model's overall performance in balancing precision and recall. Its closeness to 1 highlights the model's effectiveness in accurately identifying positive instances while minimizing incorrect predictions. The figure 19 shows the images which are classified as false negatives, false positives, true negatives, and true positives by the model.

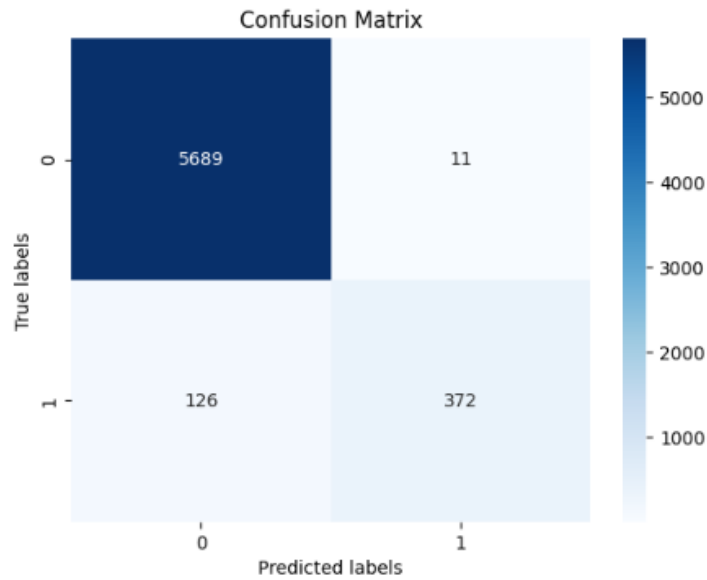


Figure 18 Confusion matrix for DOCC

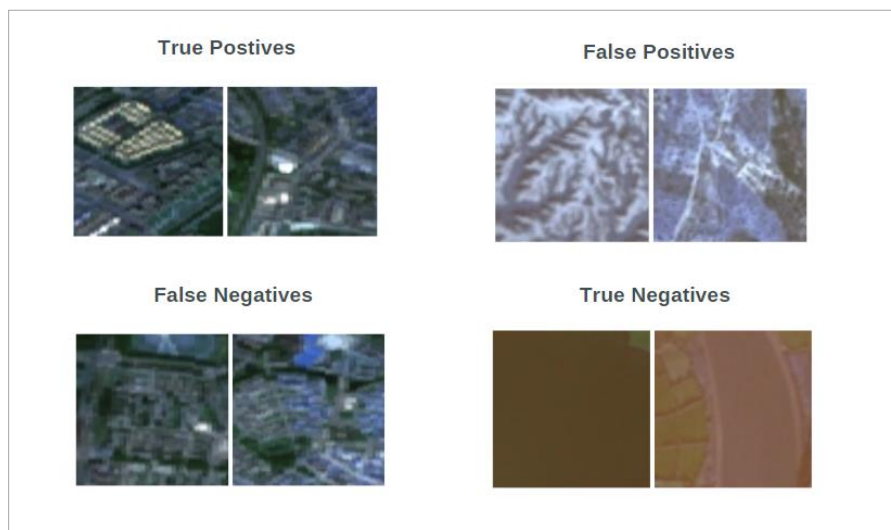


Figure 19 Detection by the DOCC model

The second phase of testing focuses on assessing the generalization capabilities of the model. In this phase, a subset of the EuroSAT dataset, which contains a mixture of Permanent crop, sea lakes and impervious surfaces like residential areas, highways, and industrial zones, is used as unseen testing images. As EuroSAT comprises a global dataset, the images represent various locations worldwide. A total of 8648 images were employed for this evaluation.

When the same model was applied to these testing images, it correctly identified residential and highway patches as impervious surfaces (positive class) while labeling other regions such as crop areas and bodies of water as negative class. The resulting confusion matrix (refer to figure 20) illustrates the model's performance, with label 1 representing the target impervious surface and label 0 denoting other classes. The matrix demonstrates a substantial number of true positives, indicating the model's proficiency in detection.

Based on these findings, we can conclude that the model exhibits good capacity to apply learned knowledge to new and unseen data. This evaluation provides valuable insights into the model's robustness and its accurate performance across diverse geographical regions.

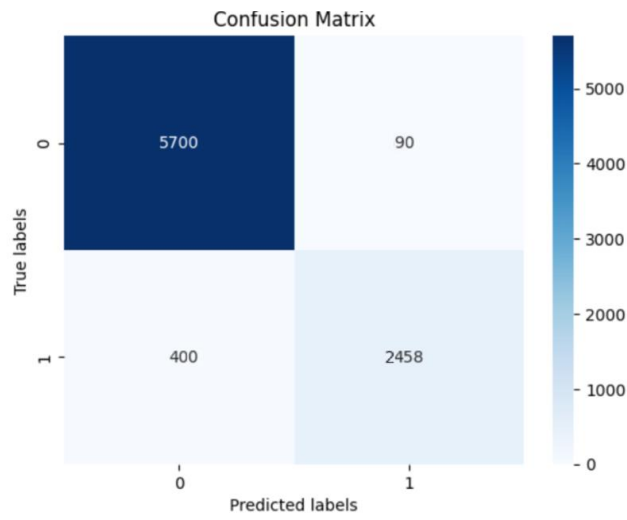


Figure 20 Confusion matrix output from second phase of testing

5.2 Results and discussion on Deep Multi-class Classification

The Deep Multi-class Classification task involved working with a dataset containing eight distinct classes, including the UIS patch. These classes are as follows: 0 - Annual crop, 1 - Forest, 2 - Herbaceous, 3 - UIS, 4 - Pasture, 5 - Permanent crop, 6 - River, and 7 - Sealake. Each number represents a specific class label. The model was built using softmax activation function to handle multi-class classification. To optimize its performance, the model underwent fine-tuning with parameters carefully set. A batch size of 32 and 25 epochs were chosen. Although it resulted in a faster learning process, it proved to be sufficient in achieving a good classification performance.

The overall F1 score achieved for the classification task was 0.9862, indicating a good level of performance. However, to facilitate comparison, the accuracy of classifying the UIS surface specifically was the focus of evaluation. As mentioned earlier label 3 represents the UIS label. The accuracy was computed for the UIS class alone with other evaluation metrics. The accuracy for UIS is the ratio of accurately classified to the instances which are not identified accurately. The accuracy was about 98 % (from figure 22).

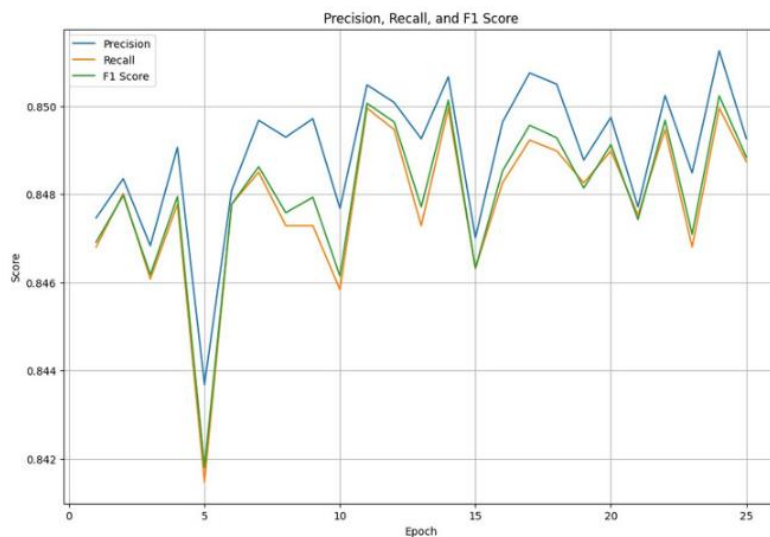


Figure 21 Graph on evaluation metrics for each epoch

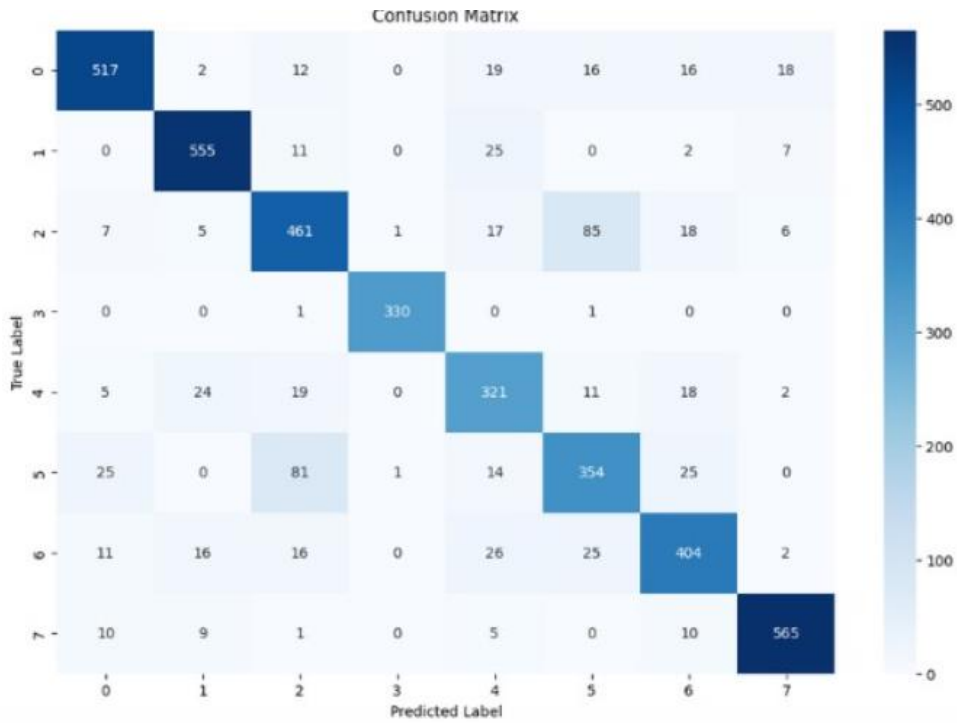


Figure 22 Confusion Matrix for multi-class classification

The graph in Figure 21 illustrates the F1 score, precision, and recall scores exclusively for the UIS class across different epochs. It is evident from the graph that these scores reached their peak shortly before the 25th epoch. Furthermore, Figure 22 displays the confusion matrix for the overall multilabel classification. Specifically focusing on Label 3, which corresponds to the UIS class, we can observe that the multiclass classifier accurately identified it with a higher number of true positives.

5.3 Comparison between One-class classifier and Multi-class classifier

One Class Classifiers have proven to be effective in handling imbalanced data (Seliya et al., 2021), making them a suitable choice when dealing with applications for detecting a single class. They leverage well-represented target training data to successfully identify anomalies. On the other hand, multi class classification requires training data from each class, which can be challenging to obtain, especially when dealing with imbalanced datasets. Despite these differences, both approaches show promising results in addressing the classification task.

When comparing the accuracy of classifying the UIS using both classifiers, it was observed that both the DOCC and the Deep Multi-Class Classification (DMCC) achieved nearly equal accuracy. The DOCC classifier achieved an accuracy of 97.8% for the UIS class, while the DMCC classifier achieved an accuracy of 98.6% for the particular UIS label.

Evaluation Metric	DOCC	DMCC(only for UIS class)
Precision	0.9713	0.9462
Recall	0.7470	0.9890
F1 Score	0.8445	0.9671
Accuracy	0.9779	0.9862

Table 3 Evaluation metrics of both DOCC and DMCC

The Table 3 presents a comparison of evaluation metrics between DOCC and the UIS class of DMCC. It is notable that the precision of DOCC outperforms DMCC, whereas the remaining metrics favor DMCC. However, considering the marginal difference between the two, we can conclude that DOCC achieves appreciable results comparable to DMCC. Upon comparing the F1 scores of DOCC and DMCC, it becomes evident that DMCC exhibits a slight improvement over DOCC. However, it is important to note that DOCC's performance is still commendable. Furthermore, the accuracy of both approaches is fairly similar to each other.

These results indicate that the DOCC approach is as efficient as DMCC in detecting the UIS without heavily relying on a large amount of labelled data unlike the multiclass classification approach. Consequently, this reduction in the need for labelled data makes it cost and time efficient, making the DOCC approach an advantageous choice for the specific tasks like UIS detection.

5.4 Results and discussion on Comparison of acquired UIS map with existing Global map

As mentioned earlier in the methodology section, we compare the UIS map generated by the DOCC model with an existing GISA map which is considered to be better in the current scenario (X. Huang et al., 2022). A subset of samples was selected, and some of them exhibited similar quality to the GISA map, as depicted in Figure 23. However, the remaining samples displayed lower quality compared to the GISA map when assessed visually. Notably, the GISA map exhibited well-defined boundaries of impervious surfaces, such as buildings, whereas the UIS map had some inaccuracies in this regard. Nevertheless, in most cases, the UIS map produced satisfactory results comparable to the GISA map.

To compare these two maps more accurate metrics like correlation coefficient was employed (X. Huang et al., 2022; X. Wang et al., 2022). Based on the calculated values, the correlation coefficient is determined to be 0.6268851409, indicating a moderate positive correlation between the two maps. This finding leads to the conclusion that there exists a good positive correlation but certain degree of variability between the two maps was also observed.

Nonetheless, it is important to note that while the GISA map has been utilized as a validation dataset, it cannot be unequivocally regarded as the ground truth, as it is also derived from recent research work. However, considering the limited availability of datasets with a 10-meter resolution and good quality, the GISA map remains a valuable resource for conducting meaningful comparisons.

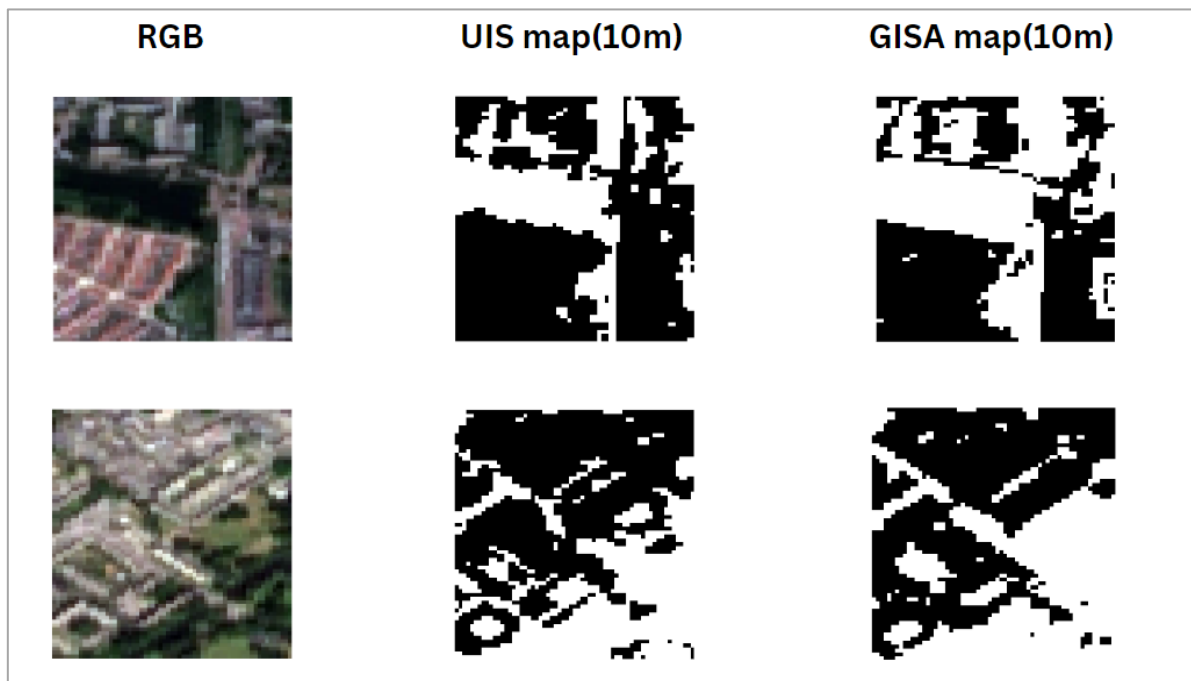


Figure 23 comparison between GISA and UIS at 10 m resolution

6. CONCLUSIONS

6.1 Conclusion

This research was conducted as a creative approach to investigate the dynamics of urban areas and the processes of urbanization in cities by developing updated labels for UIS, which provide valuable insights. A DOCC model was introduced, utilizing the integrated UIS labels obtained from a combination of remote sensing data (i.e., satellite imagery) and VGI. Through the implementation of the DOCC model, the research effectively addressed the research questions and analysed the resulting outcomes and findings.

Research Q1. How can the fusion of multiple geospatial data sources enhance the accuracy of mapping UIS? (Objective 1)

- 1.a Which remote sensing data sources are suitable for mapping UIS and why?
- 1.b What are the VGI data sources selected for mapping UIS?
- 1.c How to use VGI data sources and remote sensing data sources in an integrated way for accurate UIS mapping?

The research successfully addressed the aforementioned research question by utilizing freely available geospatial data sources such as sentinel 2 satellite imagery, Twitter geotags, and OSM data. A key aspect of this study was the development of a simple yet effective pipeline for integrating data from these different sources.

Research Q2. How can UIS (target class) be classified without taking other land cover classes into account? (Objective 2)

- 2.a How can Deep Learning be used for the One-Class Classification (OCC) approach given UIS as the target class?
- 2.b What is a suitable architecture for one-class classification for mapping UIS?
- 2.c How to prepare dataset for training and testing?

The research demonstrated that employing an OCC approach using deep learning with only a single labelled dataset for UIS mapping has a comparable efficiency to a multiclass classifier that relies on a larger labelled dataset. This highlights the potential to reduce the need for extensive labelling efforts and associated costs for similar classification tasks. The proposed DOCC uses only limited spectral features (red, green, and blue bands) in achieving an efficient UIS classification, thus showing the efficiency of the deep feature network used in the construction of the DOCC model. Therefore, the suggested DOCC architecture effectively addresses the second research question. Furthermore, the DOCC approach presented in this study has the potential to be applied to other similar one-class problems.

Research Q3. How to assess and validate the efficiency of the proposed Deep Learning One Class Classification architecture? (Objective 3)

- 3.a How can we consider spatial continuity existence in our dataset in model validation?
- 3.b How can we assess the generalization of the built model?
- 3.c How can we compare the one class and multiclass classification?

The developed model demonstrated its applicability for global applications, as the process of creating UIS labels followed a systematic pipeline that was not limited to any specific location. During the testing phase, the model was evaluated using data from EUROSAT, a global dataset spanning various regions worldwide. As a result, the evaluation performed on this diverse dataset addresses spatial continuity and generalization, taking into account the fact that the data originates from different locations. Spatial continuity refers to the model's consistent representation of impervious surface patterns across diverse locations. Evaluating the model's performance on the EUROSAT dataset, which contains data from various regions, assesses its ability to maintain spatial continuity by accurately identifying impervious surfaces regardless of location or geographic variations.

Generalization refers to the model's capacity to apply learned knowledge to new, unseen data. Testing the model on the global EUROSAT dataset determines if it can generalize its understanding of impervious surfaces beyond the specific training data. This evaluation provides insights into the model's robustness and its accurate performance on diverse geographical regions.

Furthermore, the efficiency of the DOCC was evaluated in comparison to that of a deep multi-class classifier. The findings of the study indicate that it is both feasible and efficient to map impervious surfaces in urban areas using the DOCC approach even with a limited dataset. It achieves a comparable efficiency to that of a multi-class classifier.

Furthermore, upon comparing the generated UIS map with globally available impervious surface datasets like GISA, it was observed that the UIS map exhibited a significant degree of correlation, albeit with some variability.

Thus, this approach overall provides a valuable resource for studying urban ecosystems and processes of urbanization using multiple open geospatial data sources.

6.2 Research Limitations and future works

The process of selecting tweets in the data processing pipeline can be simplified by using a single kernel or buffer instead of two. In the future, there is potential for significant advancements in the data processing side by incorporating more sophisticated and intricate methodologies (Fan et al., 2019; F. Huang et al., 2019). This study can further be extended by introducing more spectral bands in the deep feature learning phase of the DOCC model. Future studies can also explore the incorporation of other data sources, such as Synthetic Aperture Radar (SAR) or other VGI data within the same methodology.

7. ETHICAL CONSIDERATIONS, RISKS, AND CONTINGENCIES

Privacy is a key ethical consideration while handling VGI data (Mooney et al., 2017). Ethical concerns extend to areas such as legal liability, responsible use, and data quality (Fleming et al., 2018). The fusion of VGI-based information with traditional data sources stored in map databases can give rise to liability issues for people who handle and rely on digital map (Blatt, 2015). To address privacy concerns, it is crucial to have a clear understanding of the license terms associated with open source data, particularly VGI data, and employ appropriate strategies to handle privacy issues (Mooney et al., 2017). Protecting the privacy of volunteer contributors is of utmost importance for effectively managing OSM data, as it serves as an incentive for increased volunteer participation.

To ensure ethical compliance, this study will adhere to OSM's Good Practice guidelines, which are designed to promote data quality and reliability (Jaljolie et al., 2022). However, the limited temporal availability of tweets, typically spanning 5-7 days, poses a significant challenge in terms of repeatability in Twitter-related research (Granell & Ostermann, 2016). Certain methods of processing Twitter data, such as the creation of composite data without informed consent, are considered research misconduct (Webb et al., 2017).

Nevertheless, this research does not require access to tweet content or tweet IDs, effectively addressing privacy and consent concerns. Furthermore, the handling of Twitter data will strictly adhere to Twitter's policy terms and conditions to ensure ethical compliance.

LIST OF REFERENCES

- Aayog, N. (2021). Reforms in urban planning capacity in india. *Government of India, September*.
<https://www.niti.gov.in/sites/default/files/2021-09/UrbanPlanningCapacity-in-India-16092021.pdf>
- Alberti, M. (2005). The effects of urban patterns on ecosystem function. *International Regional Science Review*, 28(2), 168–192. <https://doi.org/10.1177/0160017605275160>
- Alberti, M., Booth, D., Hill, K., Coburn, B., Avolio, C., Coe, S., & Spirandelli, D. (2007). The impact of urban patterns on aquatic ecosystems: An empirical analysis in Puget lowland sub-basins. *Landscape and Urban Planning*, 80(4), 345–361. <https://doi.org/10.1016/j.landurbplan.2006.08.001>
- Andreieva, V., & Shvai, N. (2021). GENERALIZATION OF CROSS-ENTROPY LOSS. *Mobylla Mathematical Journal*, 3, 3–10. <https://doi.org/10.18523/2617-7080320203-10>
- Arnold, C. L., & Gibbons, C. J. (1996). Impervious Surface Coverage: The Emergence of a Key Environmental Indicator. *Journal of the American Planning Association*, 62(2), 243–258. <https://doi.org/10.1080/01944369608975688>
- Bah, M. D., Hafiane, A., Canals, R., & Emile, B. (2019). Deep features and One-class classification with unsupervised data for weed detection in UAV images. *2019 9th International Conference on Image Processing Theory, Tools and Applications, IPTA 2019*, 1–5. <https://doi.org/10.1109/IPTA.2019.8936091>
- Bai, Y., Sun, G., Ge, Y., Zhang, Y., & Li, Y. (2019). Mapping urban impervious surfaces by fusing optical and SAR data at decision level. *International Geoscience and Remote Sensing Symposium (IGARSS)*, 100, 6336–6339. <https://doi.org/10.1109/IGARSS.2019.8898039>
- Beckers, P., & Boschman, S. (2019). Residential choices of foreign highly skilled workers in the Netherlands and the role of neighbourhood and urban regional characteristics. *Urban Studies*, 56(4), 760–777. <https://doi.org/10.1177/0042098017741262>
- Bekker, J., & Davis, J. (2020). Learning from positive and unlabeled data: a survey. In *Machine Learning* (Vol. 109, Issue 4). Springer US. <https://doi.org/10.1007/s10994-020-05877-5>
- Blatt, A. J. (2015). *The Benefits and Risks of Volunteered Geographic Information*. 0353. <https://doi.org/10.1080/15420353.2015.1009609>
- Brodley, C. E., & Friedl, M. A. (1997). Decision tree classification of land cover from remotely sensed data. *Remote Sensing of Environment*, 61(3), 399–409. [https://doi.org/10.1016/S0034-4257\(97\)00049-7](https://doi.org/10.1016/S0034-4257(97)00049-7)
- Cadenasso, M. L., Pickett, S. T. A., & Schwarz, K. (2007). Spatial heterogeneity in urban ecosystems: Reconceptualizing land cover and a framework for classification. *Frontiers in Ecology and the Environment*, 5(2), 80–88. [https://doi.org/10.1890/1540-9295\(2007\)5\[80:SHIUER\]2.0.CO;2](https://doi.org/10.1890/1540-9295(2007)5[80:SHIUER]2.0.CO;2)
- Cervone, G., Sava, E., Huang, Q., Schnebele, E., Harrison, J., Cervone, G., Sava, E., Huang, Q., Schnebele, E., & Harrison, J. (2016). *Using Twitter for tasking remote-sensing data collection and damage assessment : 2013 Boulder flood case study Using Twitter for tasking remote-sensing data collection and damage assessment : 2013 Boulder flood case study*. January. <https://doi.org/10.1080/01431161.2015.1117684>
- Chaithanya, B. N., Swasthika Jain, T. J., Usha Ruby, A., & Parveen, A. (2021). An approach to categorize chest X-ray images using sparse categorical cross entropy. *Indonesian Journal of Electrical Engineering and Computer Science*, 24(3), 1700–1710. <https://doi.org/10.11591/ijeecs.v24.i3.pp1700-1710>
- Cheng, X., Luo, J., Shen, Z., Zhu, C., Zhang, X., & Xia, L. (2011). Estimation of impervious surface based on integrated analysis of classification and regression by using SVM. *International Geoscience and Remote Sensing Symposium (IGARSS)*, 2809–2812. <https://doi.org/10.1109/IGARSS.2011.6049864>
- Costa, S., Peters, R., Martins, R., Postmes, L., Keizer, J. J., & Roebeling, P. (2021). Effectiveness of nature-based solutions on pluvial flood hazard mitigation: The case study of the city of eindhoven (the netherlands). *Resources*, 10(3). <https://doi.org/10.3390/resources10030024>
- Deng, X., Li, W., Liu, X., Guo, Q., & Newsam, S. (2018). One-class remote sensing classification: One-class vs. Binary classifiers. *International Journal of Remote Sensing*, 39(6), 1890–1910. <https://doi.org/10.1080/01431161.2017.1416697>
- Devkota, B., Miyazaki, H., Witayangkurn, A., & Kim, S. M. (2019). Using volunteered geographic information and nighttime light remote sensing data to identify tourism areas of interest. *Sustainability (Switzerland)*, 11(17). <https://doi.org/10.3390/su11174718>
- Dreiseitl, S., Osl, M., Scheibböck, C., & Binder, M. (2010). Outlier Detection with One-Class SVMs: An Application to Melanoma Prognosis. *AMLA ... Annual Symposium Proceedings / AMLA Symposium*. *AMLA Symposium, 2010*, 172–176.
- Drusch, M., Bello, U. Del, Carlier, S., Colin, O., Fernandez, V., Gascon, F., Hoersch, B., Isola, C., Laberinti, P., Martimort, P., Meygret, A., Spoto, F., Sy, O., Marchese, F., & Bargellini, P. (2012).

- Remote Sensing of Environment Sentinel-2 : ESA 's Optical High-Resolution Mission for GMES Operational Services*, 120, 25–36. <https://doi.org/10.1016/j.rse.2011.11.026>
- Dunkel, A., Löchner, M., & Burghardt, D. (2020). Privacy-aware visualization of volunteered geographic information (VGI) to analyze spatial activity: a benchmark implementation. *ISPRS International Journal of Geo-Information*, 9(10). <https://doi.org/10.3390/ijgi9100607>
- Elwood, S., Goodchild, M. F., & Sui, D. Z. (2012). Researching Volunteered Geographic Information: Spatial Data, Geographic Research, and New Social Practice. *Annals of the Association of American Geographers*, 102(3), 571–590. <https://doi.org/10.1080/00045608.2011.595657>
- Enoguanbhor, E. C. (2023). *Assessing urban spatial patterns within the implemented urban planned areas using GIS and remote sensing data Evidence Chinedu Enoguanbhor*. May.
- Fan, W., Wu, C., & Wang, J. (2019). Improving Impervious Surface Estimation by Using Remote Sensed Imagery Combined with Open Street Map Points-of-Interest (POI) Data. *IEEE Journal of Selected Topics in Applied Earth Observations and Remote Sensing*, 12(11), 4265–4274. <https://doi.org/10.1109/JSTARS.2019.2911525>
- Fernandez, a, Garcia, S., & Herrera, F. (2011). Addressing the Classification with Imbalanced Data : Open Problems and New Challenges on Class Distribution In many applications , there exists a significant difference between the class prior Addressing the Classification with Imbalanced. *Hybrid Artificial Intelligent Systems*, 1–10.
- Fitri, M. S. N., Marena, O., Hisam, O. A., Hafiz, M. Y. M., & Izzati, A. K. N. (2022). Suitability of Open Street Map (OSM) for 1:50,000 Topographic Map. *IOP Conference Series: Earth and Environmental Science*, 1051(1), 0–13. <https://doi.org/10.1088/1755-1315/1051/1/012012>
- Fleming, S., Sedano, E., Carlin, M., Tracy, R., & Walker, J. (2018). *The Ethics of Volunteered Geographic Information for GEOINT Use. Level 4*, 27–30. <https://trajectorymagazine.com/ethics-volunteered-geographic-information-geoint-use/>
- Frias-Martinez, V., & Frias-Martinez, E. (2014). Spectral clustering for sensing urban land use using Twitter activity. *Engineering Applications of Artificial Intelligence*, 35(January), 237–245. <https://doi.org/10.1016/j.engappai.2014.06.019>
- Gao, Z., & Liu, X. (2014). Support vector machine and object-oriented classification for urban impervious surface extraction from satellite imagery. *2014 The 3rd International Conference on Agro-Geoinformatics, Agro-Geoinformatics 2014*, 2–6. <https://doi.org/10.1109/Agro-Geoinformatics.2014.6910661>
- Gašparović, M., Medak, D., Pilaš, I., Jurjević, L., & Balenović, I. (2018). Fusion of sentinel-2 and planetscope imagery for vegetation detection and monitoring. *International Archives of the Photogrammetry, Remote Sensing and Spatial Information Sciences - ISPRS Archives*, 42(1), 155–160. <https://doi.org/10.5194/isprs-archives-XLII-1-155-2018>
- Ghozatlou, O., Conde, M. H., & Datcu, M. (2022). Wavelet-Guided Deep Neural Network for Robust One-Class Classification. *Workshop on Hyperspectral Image and Signal Processing, Evolution in Remote Sensing, 2022-Septe*, 1–5. <https://doi.org/10.1109/WHISPERS56178.2022.9955071>
- Gillies, R. R., Brim Box, J., Symanzik, J., & Rodemaker, E. J. (2003). Effects of urbanization on the aquatic fauna of the Line Creek watershed, Atlanta - A satellite perspective. *Remote Sensing of Environment*, 86(3), 411–422. [https://doi.org/10.1016/S0034-4257\(03\)00082-8](https://doi.org/10.1016/S0034-4257(03)00082-8)
- Girolamo-Neto, C. D., Sato, L. Y., Sanches, I. D., Silva, I. C. O., Rocha, J. C. S., & Almeida, C. A. (2020). Object based image analysis and texture features for pasture classification in brazilian savannah. *ISPRS Annals of the Photogrammetry, Remote Sensing and Spatial Information Sciences*, 5(3), 453–460. <https://doi.org/10.5194/isprs-Annals-V-3-2020-453-2020>
- Gong, C., Shi, H., Liu, T., Zhang, C., Yang, J., & Tao, D. (2021). Loss Decomposition and Centroid Estimation for Positive and Unlabeled Learning. *IEEE Transactions on Pattern Analysis and Machine Intelligence*, 43(3), 918–932. <https://doi.org/10.1109/TPAMI.2019.2941684>
- Goodchild, M. F. (2007). Citizens as sensors: The world of volunteered geography. *GeoJournal*, 69(4), 211–221. <https://doi.org/10.1007/s10708-007-9111-y>
- Goyal, S., Raghunathan, A., Jain, M., Simhadri, H., & Jain, P. (2020). DROCC: Deep robust one-class classification. *37th International Conference on Machine Learning, ICML 2020, Part F 16814*, 3669–3679.
- Granell, C., & Ostermann, F. O. (2016). Computers , Environment and Urban Systems Beyond data collection : Objectives and methods of research using VGI and geo-social media for disaster management. *CEUS*, 59, 231–243. <https://doi.org/10.1016/j.compenvurbsys.2016.01.006>
- Grinberger, A. Y., Minghini, M., Juhász, L., Yeboah, G., & Mooney, P. (2022). OSM Science—The Academic Study of the OpenStreetMap Project, Data, Contributors, Community, and Applications. *ISPRS International Journal of Geo-Information*, 11(4). <https://doi.org/10.3390/ijgi11040230>

- Hall, D. L., Member, S., & Llinas, J. (1997). *An Introduction to Multisensor Data Fusion*. 85(1).
- Hans, L., & Koster, S. (2018). Urbanization and start-up rates in different geographies: Belgium, the Netherlands, and Sweden. *Small Business Economics*, 51(4), 1033–1054. <https://doi.org/10.1007/s11187-017-9967-2>
- He, Y. J., Zhang, J., & Zhang, Y. (2017a). Extracting urban impervious surface from GF-1 imagery using one-class classifiers. *ArXiv*.
- He, Y. J., Zhang, J., & Zhang, Y. (2017b). Extracting urban impervious surface from GF-1 imagery using one-class classifiers. *ArXiv*, May.
- Helber, P., Bischke, B., Dengel, A., & Borth, D. (2019). Eurosat: A novel dataset and deep learning benchmark for land use and land cover classification. *IEEE Journal of Selected Topics in Applied Earth Observations and Remote Sensing*, 12(7), 2217–2226. <https://doi.org/10.1109/JSTARS.2019.2918242>
- Herland, M., Bauder, R. A., & Khoshgoftaar, T. M. (2019). The effects of class rarity on the evaluation of supervised healthcare fraud detection models. *Journal of Big Data*, 6(1). <https://doi.org/10.1186/s40537-019-0181-8>
- Hong, E., & Member, G. S. (2020). *Latent Feature Decentralization Loss for One-Class Anomaly Detection*. 8. <https://doi.org/10.1109/ACCESS.2020.3022646>
- Huang, F., Yu, Y., & Feng, T. (2019). Automatic extraction of urban impervious surfaces based on deep learning and multi-source remote sensing data. *Journal of Visual Communication and Image Representation*, 60, 16–27. <https://doi.org/10.1016/j.jvcir.2018.12.051>
- Huang, X., Yang, J., Wang, W., & Liu, Z. (2022). Mapping 10 m global impervious surface area (GISA-10m) using multi-source geospatial data. *Earth System Science Data*, 14, 3649–3672. <https://doi.org/10.5194/essd-14-3649-2022>
- Jaljolje, R., Dror, T., Siriba, D. N., & Dalyot, S. (2022). Evaluating current ethical values of OpenStreetMap using value sensitive design. *Geo-Spatial Information Science*, 00(00), 1–17. <https://doi.org/10.1080/10095020.2022.2087048>
- Jha, A., Dave, M., & Madan, S. (2019). *Comparison of Binary Class and Multi-Class Classifier Using Different*. 894–903.
- Khaleghi, B., Khamis, A., Karray, F. O., & Razavi, S. N. (2013). Multisensor data fusion : A review of the state-of-the-art. *Information Fusion*, 14(1), 28–44. <https://doi.org/10.1016/j.inffus.2011.08.001>
- Kobs, K., Steininger, M., Zehe, A., & Lautenschlager, F. (n.d.). *SimLoss : Class Similarities in Cross Entropy*. 1–10.
- Lecun, Y., Bengio, Y., & Hinton, G. (2015). Deep learning. *Nature*, 521(7553), 436–444. <https://doi.org/10.1038/nature14539>
- Lei, L., Wang, X., Zhong, Y., Zhao, H., Hu, X., & Luo, C. (2021). DOCC: Deep one-class crop classification via positive and unlabeled learning for multi-modal satellite imagery. *International Journal of Applied Earth Observation and Geoinformation*, 105, 102598. <https://doi.org/10.1016/j.jag.2021.102598>
- Li, W. (2020). Mapping urban impervious surfaces by using spectral mixture analysis and spectral indices. *Remote Sensing*, 12(1). <https://doi.org/10.3390/RS12010094>
- Liu, F. E. I. T., & Ting, K. A. I. M. (2012). *Isolation-Based Anomaly Detection*. 6(1). <https://doi.org/10.1145/2133360.2133363>
- Lu, D., Li, G., Kuang, W., & Moran, E. (2014). Methods to extract impervious surface areas from satellite images. *International Journal of Digital Earth*, 7(2), 93–112. <https://doi.org/10.1080/17538947.2013.866173>
- Lu, D., Li, G., Moran, E., Batistella, M., & Freitas, C. C. (2011). Mapping impervious surfaces with the integrated use of Landsat Thematic Mapper and radar data: A case study in an urban-rural landscape in the Brazilian Amazon. *ISPRS Journal of Photogrammetry and Remote Sensing*, 66(6), 798–808. <https://doi.org/10.1016/j.isprsjprs.2011.08.004>
- Main-Knorn, M., Pflug, B., Louis, J., Debaecker, V., Müller-Wilm, U., & Gascon, F. (2017). *Sen2Cor for Sentinel-2*. October 2018, 3. <https://doi.org/10.1117/12.2278218>
- Mao, T., Fan, Y., Zhi, S., & Tang, J. (2022). A Morphological Feature-Oriented Algorithm for Extracting Impervious Surface Areas Obscured by Vegetation in Collaboration with OSM Road Networks in Urban Areas. *Remote Sensing*, 14(10). <https://doi.org/10.3390/rs14102493>
- McLaren, R. (2011). Crowdsourcing support of land administration - a partnership approach. *International Federation of Surveyors: Article of the Month*, May 2012, 12. http://www.fig.net/pub/monthly_articles/december_2011/december_2011_mclaren.html%5Chttp://www.rics.org/au/knowledge/research/research-reports/crowdsourcing-support-of-land-

- administration/
- Miao, Z., Iannelli, G. C., & Gamba, P. (2019). Using social media data to map urban areas: Ideas and limits. *International Geoscience and Remote Sensing Symposium (IGARSS)*, 5800–5803. <https://doi.org/10.1109/IGARSS.2019.8898361>
- Miao, Zelang, Xiao, Y., Shi, W., He, Y., Gamba, P., Li, Z., Samat, A., Wu, L., Li, J., & Wu, H. (2019a). Impervious Surface Classification. *IEEE Journal of Selected Topics in Applied Earth Observations and Remote Sensing*, *PP*(4), 1–14.
- Miao, Zelang, Xiao, Y., Shi, W., He, Y., Gamba, P., Li, Z., Samat, A., Wu, L., Li, J., & Wu, H. (2019b). Integration of Satellite Images and Open Data for Impervious Surface Classification. *IEEE Journal of Selected Topics in Applied Earth Observations and Remote Sensing*, *12*(4), 1120–1133. <https://doi.org/10.1109/JSTARS.2019.2903585>
- Misra, M., Kumar, D., & Shekhar, S. (2020). Urban Forestry & Urban Greening Assessing Machine Learning Based Supervised Classifiers For Built-Up Impervious Surface Area Extraction From Sentinel-2 Images. *Urban Forestry & Urban Greening*, *53*(May), 126714. <https://doi.org/10.1016/j.ufug.2020.126714>
- Mooney, P., Raimond, O., Ana-Maria, Touya, G., Juul, N. C., Alvanides, S., & Kerle, N. (2017). *Considerations of Privacy, Ethics and Legal Issues in Volunteered Geographic Information*. <https://doi.org/10.5334/bbf.f>
- Mostafa, A. H. (2021). Ensemble Model-based Weighted Categorical Cross-entropy Loss for Facial Expression Recognition. *2021 Tenth International Conference on Intelligent Computing and Information Systems (ICICIS)*, 165–171. <https://doi.org/10.1109/ICICIS52592.2021.9694244>
- Naghavi, M., Alesheikh, A. A., Hakimpour, F., Vahidnia, M. H., & Vafaeinejad, A. (2022). VGI-based spatial data infrastructure for land administration. *Land Use Policy*, *114*(January), 105969. <https://doi.org/10.1016/j.landusepol.2021.105969>
- Parekh, J. R., Poortinga, A., Bhandari, B., Mayer, T., Saah, D., & Chishtie, F. (2021). Automatic detection of impervious surfaces from remotely sensed data using deep learning. *Remote Sensing*, *13*(16). <https://doi.org/10.3390/rs13163166>
- Pauleit, S., Ennos, R., & Golding, Y. (2005). Modeling the environmental impacts of urban land use and land cover change—a study in Merseyside, UK. *Landscape and Urban Planning*, *71*(2–4), 295–310. <https://doi.org/10.1016/j.landurbplan.2004.03.009>
- Perera, P., & Patel, V. M. (2019). Learning Deep Features for One-Class Classification. *IEEE Transactions on Image Processing*, *28*(11), 5450–5463. <https://doi.org/10.1109/TIP.2019.2917862>
- Powers, D. M. W. (2020). *Evaluation: from precision, recall and F-measure to ROC, informedness, markedness and correlation*. May. <http://arxiv.org/abs/2010.16061>
- Razzak, I., Zafar, K., Imran, M., & Xu, G. (2020). Randomized nonlinear one-class support vector machines with bounded loss function to detect of outliers for large scale IoT data. *Future Generation Computer Systems*, *112*, 715–723. <https://doi.org/10.1016/j.future.2020.05.045>
- Rezaei-dastjerdehei, M. R., Mijani, A., & Fatemzadeh, E. (2020). *Addressing Imbalance in Multi-Label Classification Using Weighted Cross Entropy Loss Function*. November, 333–338. <https://doi.org/10.1109/ICBME51989.2020.9319440>
- Ruff, L., Vandermeulen, R. A., Görnitz, N., Deecke, L., Siddiqui, S. A., Binder, A., Müller, E., & Kloft, M. (2018). Deep one-class classification. *35th International Conference on Machine Learning, ICML 2018*, *10*, 6981–6996.
- Schlachter, P., Liao, Y., & Yang, B. (2019). *Deep One-Class Classification Using Intra-Class Splitting*. 100–104.
- Schmidhuber, J. (2015). Deep Learning in neural networks: An overview. *Neural Networks*, *61*, 85–117. <https://doi.org/10.1016/j.neunet.2014.09.003>
- Schmitt, M., & Zhu, X. X. (2016). *Data Fusion and Remote Sensing*. DECEMBER.
- Schnebele, E., Cervone, G., Kumar, S., & Waters, N. (2014). Real Time Estimation of the Calgary Floods Using Limited Remote Sensing Data. 381–398. <https://doi.org/10.3390/w6020381>
- Schoener, G. (2018). Urban Runoff in the U.S. Southwest: Importance of Impervious Surfaces for Small-Storm Hydrology. *Journal of Hydrologic Engineering*, *23*, 05017033. [https://doi.org/10.1061/\(ASCE\)HE.1943-5584.0001610](https://doi.org/10.1061/(ASCE)HE.1943-5584.0001610)
- SCHUELER, T. (1994). The Importance of Imperviousness. *Watershed Protection Techniques*, *1*(3), 100–101. <https://cir.nii.ac.jp/crid/1572824500088677376.bib?lang=en>
- Seliya, N., Abdollah Zadeh, A., & Khoshgoftaar, T. M. (2021). A literature review on one-class classification and its potential applications in big data. In *Journal of Big Data* (Vol. 8, Issue 1). Springer International Publishing. <https://doi.org/10.1186/s40537-021-00514-x>

- Shao, Z., Sumari, N. S., Portnov, A., Ujoh, F., & Mandela, P. J. (2021). Geo-spatial Information Science Urban sprawl and its impact on sustainable urban development : a combination of remote sensing and social media data. *Geo-Spatial Information Science*, 24(2), 241–255. <https://doi.org/10.1080/10095020.2020.1787800>
- Soliman, A., Soltani, K., Yin, J., Padmanabhan, A., & Wang, S. (2017). Social sensing of urban land use based on analysis of Twitter users' mobility patterns. *PLoS ONE*, 12(7), 1–16. <https://doi.org/10.1371/journal.pone.0181657>
- Stasolla, M., & Gamba, P. (2008). Spatial indexes for the extraction of formal and informal human settlements from high-resolution SAR images. *IEEE Journal of Selected Topics in Applied Earth Observations and Remote Sensing*, 1(2), 98–106. <https://doi.org/10.1109/JSTARS.2008.921099>
- Steiger, E., Westerholt, R., Resch, B., & Zipf, A. (2015). Twitter as an indicator for whereabouts of people? Correlating Twitter with UK census data. *Computers, Environment and Urban Systems*, 54, 255–265. <https://doi.org/10.1016/j.compenvurbsys.2015.09.007>
- Strobel, J. R. A., de Carvalho, M. A. G., Gonçalves, R., Pedroso, C. B., dos Reis, M. N., & Martins, P. S. (2018). Quantitative image analysis of acoustic tomography in woods. *European Journal of Wood and Wood Products*, 76(5), 1379–1389. <https://doi.org/10.1007/s00107-018-1323-y>
- Sun, Z., Du, W., Jiang, H., Weng, Q., Guo, H., Han, Y., Xing, Q., & Ma, Y. (2022). Global 10-m impervious surface area mapping: A big earth data based extraction and updating approach. *International Journal of Applied Earth Observation and Geoinformation*, 109(October 2021), 102800. <https://doi.org/10.1016/j.jag.2022.102800>
- Tan, W., Liao, R., Du, Y., Lu, J., & Li, J. (2015). Improving urban impervious surface classification by combining Landsat and PolSAR images: A case study in Kitchener-Waterloo, Ontario, Canada. *International Geoscience and Remote Sensing Symposium (IGARSS), 2015-Novem*, 1917–1920. <https://doi.org/10.1109/IGARSS.2015.7326169>
- Tian, Y., Chen, H., Song, Q., & Zheng, K. (2018). A novel index for impervious surface area mapping: Development and validation. *Remote Sensing*, 10(10). <https://doi.org/10.3390/rs10101521>
- Torres, R., Snoeij, P., Geudtner, D., Bibby, D., Davidson, M., Attema, E., Potin, P., Rommen, B. Ö., Floury, N., Brown, M., Traver, I. N., Deghaye, P., Duesmann, B., Rosich, B., Miranda, N., Bruno, C., L'Abbate, M., Croci, R., Pietropaolo, A., ... Rostan, F. (2012). GMES Sentinel-1 mission. *Remote Sensing of Environment*, 120, 9–24. <https://doi.org/10.1016/j.rse.2011.05.028>
- Turney, P. D. (2014). *NRC Publications Archive (NPArc) Archives des publications du CNRC (NPArc) Types of Cost in Inductive Concept Learning. December 2002.*
- van der Linden, S., & Hostert, P. (2009). The influence of urban structures on impervious surface maps from airborne hyperspectral data. *Remote Sensing of Environment*, 113(11), 2298–2305. <https://doi.org/10.1016/j.rse.2009.06.004>
- Wang, Shuo, & Yao, X. (2012). Multiclass imbalance problems: Analysis and potential solutions. *IEEE Transactions on Systems, Man, and Cybernetics, Part B: Cybernetics*, 42(4), 1119–1130. <https://doi.org/10.1109/TSMCB.2012.2187280>
- Wang, Sishi, Tan, X., & Fan, F. (2023). Changes in Impervious Surfaces in Lhasa City , a Historical City on the Qinghai – Tibet Plateau. *Sustainability*, 15, 5510. <https://doi.org/10.3390/su15065510>
- Wang, X., Liu, C., Lv, G., & Xu, J. (2022). *Integrating Multi-Source Remote Sensing to Assess Forest Aboveground Biomass in the Khingan Mountains of North-Eastern China Using Machine-Learning Algorithms.*
- Wang, Y., & Li, M. (2022). Urban Impervious Surface Automatic Threshold Detection Model Derived from Multitemporal Landsat Images. *IEEE Transactions on Geoscience and Remote Sensing*, 60. <https://doi.org/10.1109/TGRS.2021.3089581>
- Webb, H., Jirotko, M., Stahl, B. C., Housley, W., Edwards, A., Williams, M., Procter, R., Rana, O., & Burnap, P. (2017). The ethical challenges of publishing Twitter data for research dissemination. *WebSci 2017 - Proceedings of the 2017 ACM Web Science Conference, June*, 339–348. <https://doi.org/10.1145/3091478.3091489>
- Weiss, G. M., & Provost, F. (2014). *Learning When Training Data are Costly : The Effect of Class Distribution on Tree Induction Learning When Training Data are Costly : The Effect of Class Distribution on Tree Induction.* May. <https://doi.org/10.1613/jair.1199>
- Weng, Q. (2012). Remote sensing of impervious surfaces in the urban areas: Requirements, methods, and trends. *Remote Sensing of Environment*, 117, 34–49. <https://doi.org/10.1016/j.rse.2011.02.030>
- Wiedemann, A., & Beckmann, S. (2016). Quality aspects of aerial digital orthophotos, the producers point of view. *International Archives of the Photogrammetry, Remote Sensing and Spatial Information Sciences - ISPRS Archives*, 41(July), 449–453. <https://doi.org/10.5194/isprsarchives-XLI-B2-449-2016>

- Wu, M., Zhao, X., Sun, Z., & Guo, H. (2019). A Hierarchical Multiscale Super-Pixel-Based Classification Method for Extracting Urban Impervious Surface Using Deep Residual Network from WorldView-2 and LiDAR Data. *IEEE Journal of Selected Topics in Applied Earth Observations and Remote Sensing*, 12(1), 210–222. <https://doi.org/10.1109/JSTARS.2018.2886288>
- Xiang, D., Tang, T., Ban, Y., Su, Y., & Kuang, G. (2016). Unsupervised polarimetric SAR urban area classification based on model-based decomposition with cross scattering. *ISPRS Journal of Photogrammetry and Remote Sensing*, 116, 86–100. <https://doi.org/10.1016/j.isprsjprs.2016.03.009>
- Xu, R., Liu, J., & Xu, J. (2018). Extraction of high-precision urban impervious surfaces from sentinel-2 multispectral imagery via modified linear spectral mixture analysis. *Sensors (Switzerland)*, 18(9), 1–15. <https://doi.org/10.3390/s18092873>
- Xu, Z., Mountrakis, G., & Quackenbush, L. J. (2017). Impervious surface extraction in imbalanced datasets: integrating partial results and multi-temporal information in an iterative one-class classifier. *International Journal of Remote Sensing*, 38(1), 43–63. <https://doi.org/10.1080/01431161.2016.1259677>
- Yan, Y., Wei, W., Li, J., & Zhang, Y. (2018). URBAN IMPERVIOUS SURFACE EXTRACTION BASED ON THE INTEGRATION OF REMOTE SENSING IMAGES AND SOCIAL MEDIA DATA Guangdong Provincial Key Laboratory of Urbanization and Geo-simulation , ShaanXi Provincial Key Laboratory of Speech and Image Information Processi. *IEEE International Geoscience and Remote Sensing Symposium, Valencia, Spain, 2018*, Pp. 8861-8864, 8865–8868.
- Zhang, J. (2010). *Multi-source remote sensing data fusion : status and trends*. 9832. <https://doi.org/10.1080/19479830903561035>
- Zhao, H., Zhong, Y., Wang, X., Hu, X., Luo, C., Boitt, M., Piironen, R., Zhang, L., Heiskanen, J., & Pellikka, P. (2022). Mapping the distribution of invasive tree species using deep one-class classification in the tropical montane landscape of Kenya. *ISPRS Journal of Photogrammetry and Remote Sensing*, 187(March), 328–344. <https://doi.org/10.1016/j.isprsjprs.2022.03.005>

Annexes:

Attribute with fields of counts and buffer_count:

	x	y	count	geometry	buffer_counts	buffer
0	4.950370	52.348906	237	POINT (4.950 52.349)	39	POLYGON ((4.955 52.349, 4.955 52.348, 4.955 52...
1	4.669694	52.230625	17780	POINT (4.670 52.231)	13	POLYGON ((4.675 52.231, 4.675 52.230, 4.675 52...
2	4.863980	52.154190	32	POINT (4.864 52.154)	3	POLYGON ((4.869 52.154, 4.869 52.154, 4.869 52...
3	5.221907	51.960649	4	POINT (5.222 51.961)	34	POLYGON ((5.227 51.961, 5.227 51.960, 5.227 51...
4	4.531620	51.945885	1228	POINT (4.532 51.946)	7	POLYGON ((4.537 51.946, 4.537 51.945, 4.537 51...
...
1048474	5.471882	52.501944	2	POINT (5.472 52.502)	31	POLYGON ((5.477 52.502, 5.477 52.501, 5.477 52...
1048486	5.796218	51.817610	1	POINT (5.796 51.818)	14	POLYGON ((5.801 51.818, 5.801 51.817, 5.801 51...
1048512	5.862974	51.826739	1	POINT (5.863 51.827)	63	POLYGON ((5.868 51.827, 5.868 51.826, 5.868 51...
1048526	4.913177	52.399194	1	POINT (4.913 52.399)	85	POLYGON ((4.918 52.399, 4.918 52.399, 4.918 52...
1048561	4.862486	52.375549	3	POINT (4.862 52.376)	117	POLYGON ((4.867 52.376, 4.867 52.375, 4.867 52...

119031 rows × 6 columns

Snippet of Evaluation metrics of the DOCC:

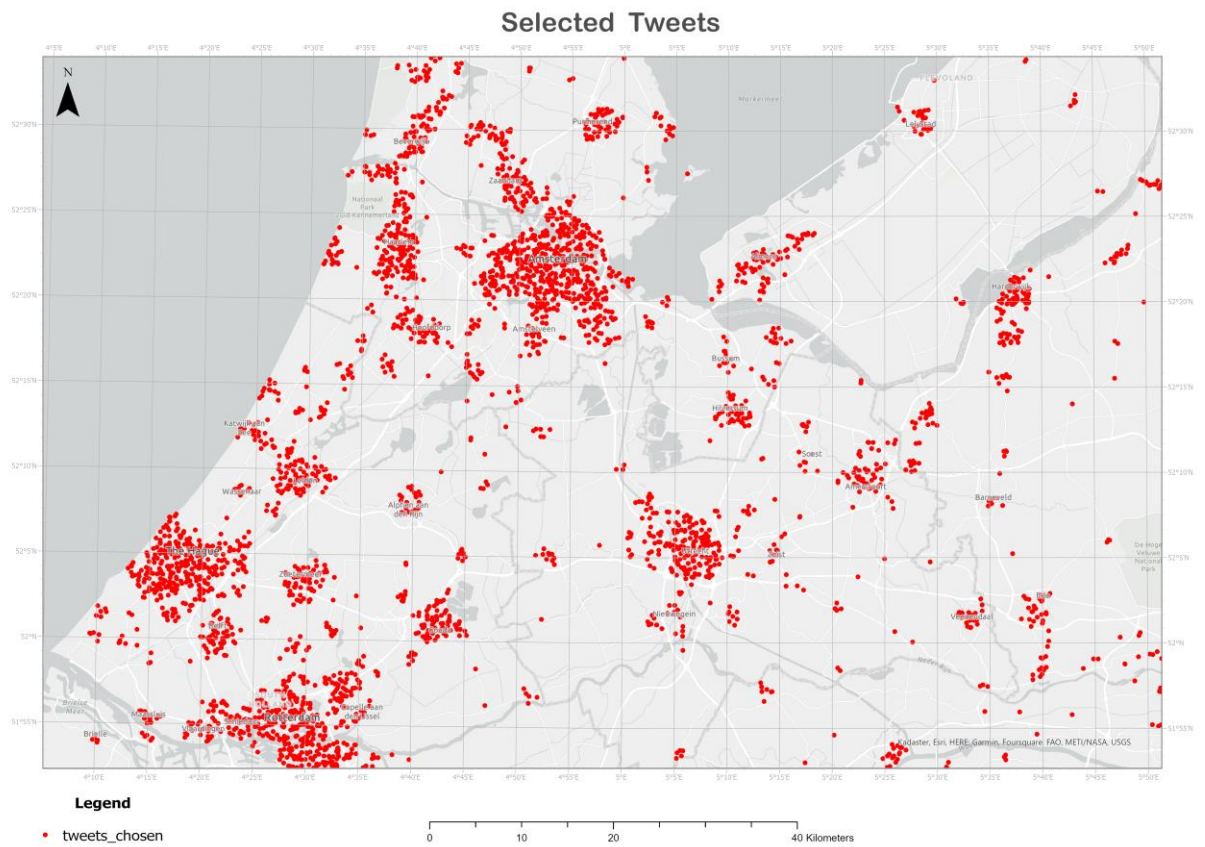
```
Precision: 0.9712793733681462
Recall: 0.7469879518072289
F1 Score: 0.8444948921679909
Specificity: 0.9980701754385964
Accuracy: 0.9778960955146822
```

Snippet of Evaluation metrics of the DMCC:

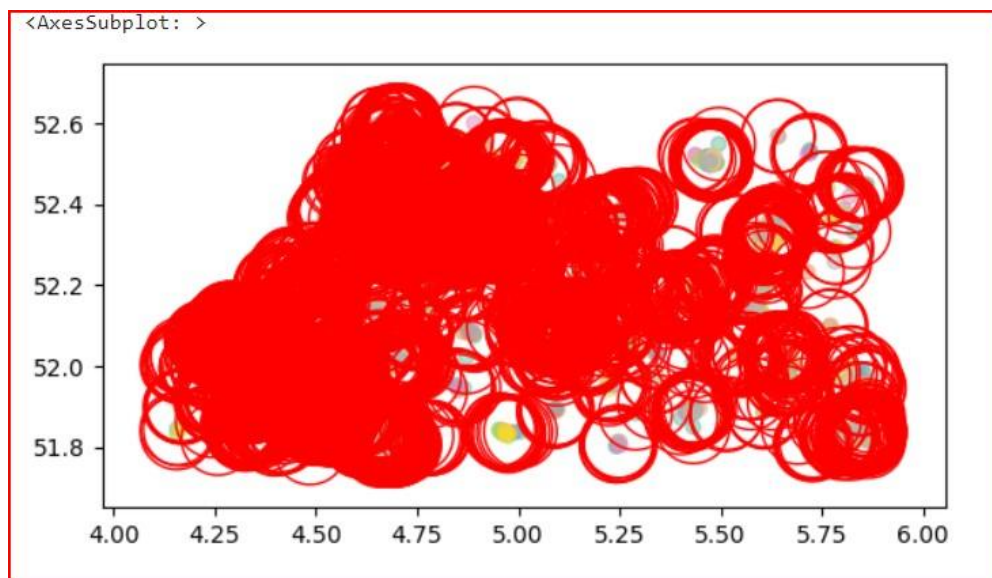
```
Accuracy for class 3 UIS: 0.9862
Precision for class 3 UIS: 0.9462
Recall for class 3 UIS: 0.9890
F1 Score for class 3 UIS: 0.9671
```

Annexes:

Tweets selected after condition 1:



Buffer_2 with 10,000 meters:



Comparison between GMIS and UIS at 30 m resolution:

